Available online at www.sciencedirect.com
ScienceDirect
Gondwana Research 12 (2007) 202–227
www.elsevier.com/locate/gr

GR Focus

The Neoproterozoic supercontinent Palaeopangaea

J.D.A. Piper

Geomagnetism Laboratory, Department of Earth and Ocean Sciences, University of Liverpool, Liverpool L69 7ZE, UK

Received 15 November 2005; accepted 10 October 2006
Available online 14 December 2006

Abstract

The Rodinia hypothesis for the Neoproterozoic Supercontinent reconstruction is associated with five major problems: (i) The palaeomagnetic test requires continental break-up hundreds of millions of years before the geological evidence for this event is recognised near the dawn of the Cambrian. (ii) The reconstruction separates cratons with strong Late Archaean–Early Proterozoic affinities by large distances and then recombines them into Gondwana by early Phanerozoic times. (iii) The stratigraphic correlation, upon which it was originally based, incorporates successions dated ~850–550 Ma during which interval palaeomagnetic data fail to predict continuity between Western North America, Australia and South China. (iv) The protracted history of break-up from 800–550 Ma is in conflict with the global subsidence record of passive margins defining initial continental break-up at ~600 Ma and diverse isotopic/environmental signatures concentrated between 600–500 Ma. (v) It predicts no intrinsic link (such as a peripheral subduction zone) to large-scale mantle constraining forces.

The Palaeopangean reconstruction, formulated a decade before Rodinia, was defined by correlation of ~2700–600 Ma palaeomagnetic poles and predicted a quasi-rigid configuration peripherally modified by continental break-up late in the Mesoproterozoic, with a secondary quasi-rigid Neoproterozoic reconstruction surviving until ca. 600 Ma. Since Palaeopangaea addresses each of the above problems, it is re-evaluated here using the 1300–500 Ma database to March 2005, which has been greatly expanded and revised since the original proposition. Poles are shown to conform to a quasi-rigid reconstruction embracing a single APW path comprising the Gardar Track, the Keweenawan Track, the Grenville–Sveconorwegian Loop and the Franklin–Adelaide Track. The reconstruction is confirmed by sequential conformity of the high precision dated anchor poles to the APW path from 1250 Ma until 600 Ma. At this point the poles scatter and identify the geologically defined global continental break-up shortly before the dawn of the Cambrian. The key test between Rodinia and Palaeopangaea embraces the interval 800–600 Ma when all Rodinia models require differential movements between the continental blocks. The database has now expanded sufficiently to show that the poles assigned to this interval actually plot sequentially along a single APW path. Major implications of the Palaeopangaean reconstruction are: (a) continental break-up took place when the geological, geochemical and isotopic evidence predict it near the end of Neoproterozoic times; (b) The Late Archaean–Early Proterozoic cratonic nuclei of Gondwana held the proximities in Neoproterozoic times that they retained until Mesozoic times; (c) The ~1100 Ma Grenville-age orogenic belts were linked as an en echelon circum-continental system conforming to the shape of the supercontinent; some were Andean in character and others were essentially intracratonic; (d) Late Neoproterozoic subduction was peripheral and focussed symmetrically within the instep between the two wings of the reconstruction; (e) Palaeopangaea possessed a symmetrical, crescent and hemispheric shape analogous to the Phanerozoic supercontinent (Neo)pangaea. Like the latter supercontinent, it appears to have been constrained by large-scale mantle convection related to the geoid form.

Keywords: Supercontinents; Palaeomagnetism; Palaeopangaea; Rodinia; Geoid; Neoproterozoic; Cambrian continental break-up; Apparent polar wander

Contents

1. Introduction . . . 203
2. The Rodinia proposition in retrospect . . . 203
3. The Palaeopangaean reconstruction . . . 205
   3.1. The palaeomagnetic test . . . 206

E-mail address: sg04@liverpool.ac.uk.

doi:10.1016/j.gr.2006.10.014

3.2. The Mackenzie–Gardar track, 1300–1140 Ma . . . 218
3.3. The Keweenawan track and Grenville–Sveconorwegian loop, 1140–800 Ma. . . . 219
3.4. The Franklin–Adelaide track, 800–600 Ma . . . 220
3.5. The Eocambrian continental break-up . . . 220
4. Geological and geophysical implications . . . 221
4.1. Continental shape and relationship to the Geoid . . . 221
4.2. Meso–Neoproterozoic orogeny and sedimentation . . . 222
4.3. Late Neoproterozoic continental break-up and isotopic signatures . . . 223
5. Conclusions . . . 225
Acknowledgements . . . 225
References . . . 225

1. Introduction

The concept of a Neoproterozoic Supercontinent is embraced by a range of petrologic, geochemical and tectonic evidence for Proterozoic continentality (e.g. Ronov, 1968; Engel et al., 1974; McLennan and Taylor, 1983; Piper, 1987) terminated by a global episode of continental break-up beginning shortly before Cambrian times (Bond et al., 1984; Conway Morris, 1987). McMenamin and McMenamin (1990) highlighted the extraordinary environmental and biological implications of this latter event in formulating their proposed supercontinent "Rodinia". The most influential concept supposedly constraining the geometrical form of this supercontinent has been a proposed correlation between Neoproterozoic sedimentary successions in Eastern Australia, South China and Western North America (e.g. Eisbacher, 1985; Bell and Jefferson, 1987). This proposition was specifically developed by Moores (1991) and Dalziel (1991) and extended by Hoffman (1991) who correlated ~1100 Ma 'Grenville' orogenic belts to flesh out a supercontinent model that became almost universally accepted during the subsequent decade and is now associated with the name "Rodinia".

A difficulty with this reconstruction was recognised when Powell et al. (1993) were unable to demonstrate a palaeomagnetic correlation conforming to the Rodinian reconstruction between Australia and Laurentia after 740 Ma. They were thus forced to postulate continental break-up well before the great Eocambrian event identified from the geological record (Bond et al., 1984; Piper, 1987; Conway Morris, 1987 and Section 4.3). Even a proposed date for break-up as late as ~740 Ma depended critically on a pole from the Australian 'YB' dykes which have since been shown to have a remanence unrelated to these times (Halls and Wingate, 2001). However most authors have preferred to adapt the history of Rodinia to an early break-up event by retaining a distribution of shields around a Laurentian core and matching selected poles to derive transient reconstructions (e.g. Meert and Torsvik, 2003). An early putative break-up is accommodated by invoking transitional supercontinents culminating in a fusion of East and West Gondwana by Early Palaeozoic times (e.g. Idnurm and Giddings, 1995; Li et al., 1995; Smethurst et al., 1998; Weil et al., 1998; Meert and Torsvik, 2003).

Whilst there have been challenges to specific aspects of the archetypal Rodinia reconstruction, mainly based on palaeomagnetic data (e.g. Evans et al., 2000; Wingate et al., 2002), most authors remain committed to its general proposition. Hence the present perception of the Neoproterozoic Supercontinent (retaining for this the name 'Rodinia') in the minds of most Earth Scientists remains one with a Laurentian core and Australia–Antarctica–India–South China arranged around its western margin and the other Precambrian shields distributed around the remaining perimeter, and specifically with South American cratons adjacent to the Grenville belt of eastern North America (Weil et al., 1998).

In this paper I test an alternative model that addresses the difficulties with the Rodinia reconstruction noted above; this is Palaeopangaea, a hypothesis proposed a decade before Rodinia (Piper, 1982, 1987). Although variants of the Rodinian reconstruction have multiplied in recent years, it is possible to make a definitive palaeomagnetic test between the two propositions during the late Precambrian interval 800–600 Ma because all Rodinia models invoke differential continental movements during these times whilst Palaeopangaea predicts continental integrity until ~600 Ma. The palaeomagnetic database has now expanded to a point at which high precision (and also lesser rank) poles assigned to this interval are seen to conform to a single path. An outcome of this test is to show that the form of the Neoproterozoic Supercontinent was close to Palaeopangaea as defined in 1982 and is actually similar to the original form of Rodinia as proposed by McMenamin and McMenamin in 1989.

2. The Rodinia proposition in retrospect

The present palaeogeographic perception of Rodinia dates from the proposition that Neoproterozoic successions of Western North America, Eastern Australia and South China have comparable lithostratigraphies that exhibit a large scale three fold repetition suggesting close spatial relationships (Eisbacher, 1985; Bell and Jefferson, 1987). This hypothesis has prompted some detailed stratigraphic and tectonic correlations (Young, 1992; Burrett and Berry, 2000) and numerous other authors have developed the wider correlation with East Antarctica and South China (e.g. Dalziel, 1991; Li and Powell,

1993; Li et al., 1995; Dalziel, 1997; Powell and Pisarevsky, 2002). Also influential in defining the popular form of Rodinia has been a supposed correlation of ~1100 Ma ("Grenville") orogenic belts (Hoffman, 1991). An extension of this facet of the reconstruction is the supposition that the type Grenville belt at the SE margin of Laurentia is of collisional rather than Andean origin and is to be paired with the northwest margin of the Amazonian margin of South America during the latter part of the Proterozoic eon as proposed by Dalziel (1992) and adopted by numerous authors since.

Specific problems with the reconstruction formulated on the above precepts are itemised into four sections below:

(i) The stratigraphic successions that form the basis of the Australia–South China–Western Laurentia correlation are dated ~850–550 Ma and require palaeomagnetic support for the palaeogeographic link during these times. However, this test has manifestly failed during this interval (Powell et al., 1993; Meert and Torsvik, 2003). The only possible palaeomagnetic correlations satisfying the Rodinia premise predate the stratigraphic successions yielding the palaeogeographic hypothesis and hence provide no direct support for it.

(ii) A geological case based on tectonic trends, dyke swarms, a basic igneous event comparable to the Franklin episode (~740 Ma), and a Tommotian subsidence history of passive margins has been developed to link the Siberian Shield with the western margin of Laurentia (Sears and Price, 1978, 2000). This alternative interpretation would require that Siberia rather than Australia–South China–East Antarctica occupied this position during Neoproterozoic times.

(iii) The wider development of Rodinia derived by correlating ~1100 Ma orogenic belts (Hoffman, 1991) produces a large separation of the Indian cratons (Singhbhum and Dharwar with the latter incorporating and Karnataka) and Australian cratons (Kilbaran and Pilbara) on the one hand and southern African cratons (Kaapvaal, Zimbabwe) on the other. There are strong geological similarities of Late Archaean–Early Proterozoic age between these cratons (e.g. Rogers, 1996; Wingate, 1998; Zegers et al., 1998; Nelson et al., 1999) and the reconstruction of the Gondwana supercontinent, which is not substantially in dispute, requires that they preserved their proximities until the Mesozoic break-up of Pangaea. Attempts to overcome this problem by invoking models to recombine the nuclei by Early Palaeozoic times have been proposed (Dalziel, 1992) and involve the rapid pivotal opening of large oceans in Neoproterozoic times for which there is little geological and no isotopic evidence (as addressed in Section 4.3). The invocation of transitional supercontinents such as "Pannotia" (Powell, 1995) is inherently unsatisfactory for the same reason and is unable to address why the Kaapvaal and Pilbara nuclei were in proximity in Archaean and Mesozoic times but widely separated in Neoproterozoic times.

(iv) Most models proposing an Amazonia–Laurentia correlation have required removal of the Fennoscandian Shield from a relatively well-constrained position against eastern Laurentia (Patchett et al., 1978; Piper, 1980a; Stearn and Piper, 1984; Elming and Mattsson, 2001). Late Archaean–Mesoproterozoic reconstructions of the Laurentian and Fennoscandian Shields show them in close proximity with tectonic lineaments terminating in the Grenville–Sveconorwegian orogenic belt and testable until the ~1250 Ma Jotnian and Mackenzie palaeomagnetic poles (e.g. Patchett and Bylund, 1977; Piper, 1980a,b; Buchan et al., 2000; Elming and Mattsson, 2001). Subsequent correlation of the Grenville and Sveconorwegian palaeomagnetic loops (~1050–850 Ma) identifies break-up and rotation between these shields at ~1100–1050 Ma and a Neoproterozoic reconstruction, again with the Fennoscandian Shield close to the Grenville margin (Patchett et al., 1978; Piper, 1980a; Stearn and Piper, 1984). This correlation is destroyed by Rodinia reconstructions that shift Fennoscandia northwards around the margin of Greenland to make room for the South American shields (e.g. Dalziel, 1997; Smethurst et al., 1998). It is largely preserved by the more conservative reconstructions of Hoffman (1991) and Weil et al. (1998) which place the Amazonian Shield in the instep between Laurentia and Fennoscandia although this implies that the reconstruction was only achieved after rotation of Fennoscandia at ~1000 Ma. In contrast the Grenville orogenic belt had a long tectonic history embracing an interval of at least 300 Ma prior to the ~1100 Ma peak of orogenesis (Hanmer et al., 2000) and there is no unique correlation with the Rondonia–Sunsas belt of the NW Amazonian margin. Attempts to match Laurentia and Amazonia as paired forelands to the Grenville Belt also appear to be comparing shields of contrasting pedigree (De Wit et al., 1999): West Africa and South America are linked by common metallogenic tin and wolframite provinces, including Grenville-age zones, whereas these metals are entirely absent in North America. In contrast the geological links between Laurentia and Fennoscandia are well established and have been invoked by many other palaeomagnetic comparisons (e.g. Buchan et al., 2000; Pesonen et al., 2003). The most important problem with the placement of Amazonia against the Grenville margin of Laurentia is the geodynamic difficulty of transferring South America to the opposite side of the Rodinia reconstruction in order to assemble it adjacent to the western side of the African shields in Gondwana by Early Palaeozoic times. Major left-lateral transpression to achieve the Gondwana configuration by Early Palaeozoic times is a key feature of all Rodinia models (e.g. Hoffman, 1991; Dalziel, 1997) and it is at least curious that the South American shields should somehow have defied this trend especially since a Precambrian geological link with western Africa is widely acknowledged (e.g. Trompette, 1997).

(v) The most serious defect of the Rodinia hypothesis remains the failure to accommodate the widespread break-up of continental crust at the end of the

Neoproterozoic. This event is a comprehensive and integral feature of the geological record. It is embraced by evidence for rifting and dyke injection, alkaline magmatism, widespread transition from fluviatile to marine sedimentation, and the worldwide subsidence of passive margins at ~600–560 Ma (Doig, 1970; Bond et al., 1984; Conway Morris, 1987; Piper, 1987); it is also seen as a distinctive isotopic signature in the oceanic record (Holser, 1977; Knoll et al., 1986; Conway Morris, 1987; Veizer, 1989). This was a temporally concentrated episode at ~600–560 Ma rather than a ~800–550 Ma temporally distributed one, and discussion in terms of break-up of the last vestiges of Rodinia is clearly unsatisfactory (e.g. Meert and Torsvik, 2003).

3. The Palaeopangaean reconstruction

The core tenets of the Palaeopangaean reconstruction were invoked in the early 1980's (Piper, 1980a, 1982, 1983a,b) from conformity of palaeomagnetic poles over a long interval of geological time with a single and relatively simple apparent polar wander (APW) path. It was always acknowledged that this did not require that the crust was then a single integral unit; the presence of Precambrian ophiolites and an obviously dynamic crust showed that this could not have been the case. Instead it implied that the continental crust was constrained to a single quasi-rigid geometry in palaeomagnetically-resolvable terms as constrained by mantle driving forces. This observation provided a general explanation for the distinctive Proterozoic lithostratigraphic, geochemical, metallogenic and isotopic signatures of the Proterozoic eon (e.g. Ronov, 1968; Engel et al., 1974; Hutchinson, 1981; McLennan and Taylor, 1983; Piper, 1987; Veizer, 1989). The reconstruction was shown to be consistent with an axial alignment of many tectonic trends, as well as regional secular cooling and consolidation of the crust defined by the contraction of anorthosite–rapakivi magmatism during Mesoproterozoic times (Piper, 1987).

A feature of the palaeomagnetic analysis was a break-up and reorganisation of peripheral parts of the reconstruction late in Mesoproterozoic times (Fig. 1). The core correlation between the results from southern African shields and Laurentia appeared to be palaeomagnetically invariant from ~2700 Ma until the dawn of the Cambrian whereas a primitive reconstruction incorporating Fennoscandia, Australia and India could not be matched to Neoproterozoic poles and implied movement between these blocks late in Mesoproterozoic times. A link between this event and the widespread Mackenzie and related large igneous province (LIP) events was inferred and at this point

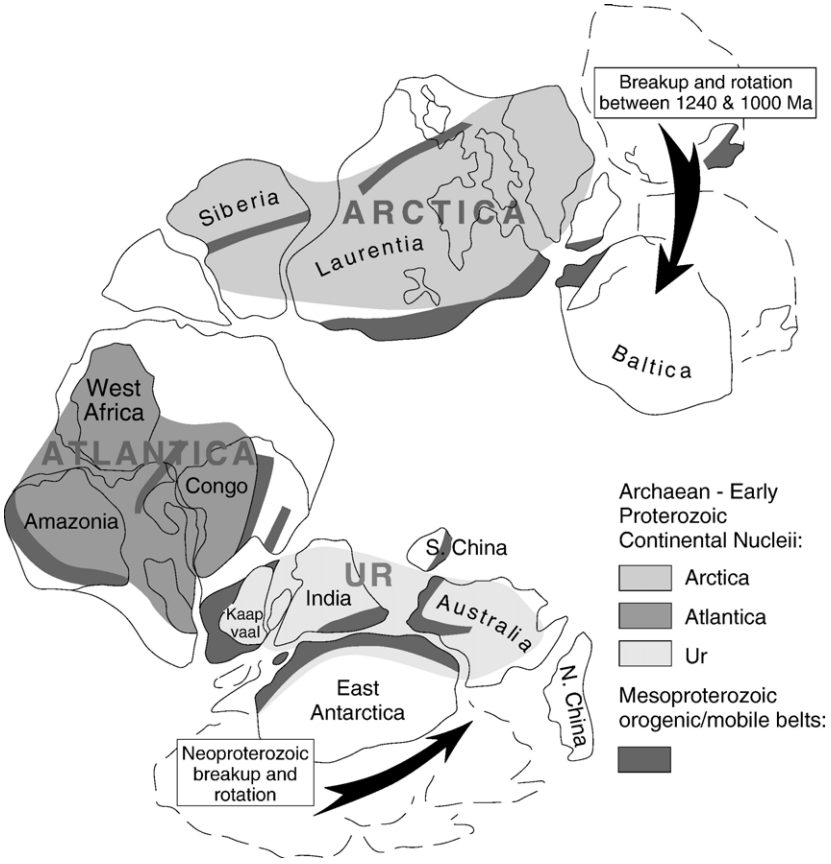


Fig. 1. Diagrammatic reconstruction of Palaeopangaea after Piper (1982, 2000) indicating generalised Late Mesoproterozoic–Early Neoproterozoic movements from a Palaeo–Mesoproterozoic precursor. The Archaean–Palaeoproterozoic continental nuclei are inferred from distinct temporal histories of cratonic stabilisation and supracrustal development (Rogers and Santosh, 2004) and support proximities, but not necessarily configurations, shown here. It is argued in this paper that the configurations of West African, Sao Francisco–Rio de la Plata and Gutana–Amazonian nuclei were somewhat different from the Gondwana configurations shown prior to Pan African orogenesis.

both Rodinian and Palaeopangaean hypotheses have a facet in common: in Rodinia models this event is usually seen as coincident with formation of the supercontinent whereas in Palaeopangaea it is seen as defining the reorganisation of a constrained continental body (Fig. 1).

3.1. The palaeomagnetic test

A palaeomagnetic test between Rodinia and Palaeopangaea several years ago compared ~1150–550 Ma palaeomagnetic data (Piper, 2000) and highlighted the failure of the former reconstruction after ~800 Ma. The Rodinia models have now diversified so much that it is no longer feasible to make a straightforward comparison between the two propositions. It is however, possible to make a definitive test in the late Precambrian interval 800–600 Ma because all Rodinia models without exception invoke differential movements between continental blocks during these times. This is necessitated by divergence of Gondwana and Laurentian APW paths after ~800 Ma (Powell et al., 1993; Meert and Torsvik, 2003).

In this paper the case for Palaeopangaea is commenced at ~1300 Ma to embrace the putative break-up event late in Mesoproterozoic times and the Global Palaeomagnetic Database (GPDB) updated to March 2005 is the primary data source. Since attempts to reference each determination have now grown totally unwieldy, poles are linked to their reference numbers in the database and the compilation of Table 1 includes determinations from the interval 1300–500 Ma based on demagnetisation studies of $N > 15$ samples and $\alpha_{95} \leq 15°$ with ages estimated to be better than ±150 Ma. Within these four criteria data illustrating a Quality Factor ≥2 are included although results described as "superseded" in the GPDB are excluded. To aid the definition of APW some mean pole positions from each shield division are calculated and assigned an average age when consecutive groups of poles fall into similar positional and age groups. These are shown in bold typeface in Table 1 and extended to include anchor poles constrained by high precision age dates but otherwise unsupported by poles of similar age plotting nearby.

Any geometrical model based primarily on palaeomagnetic data must stand or fall from the agreement, or otherwise, of the key anchor poles linked to precision age dates; this point has been stressed by Buchan et al. (2000) and many others. During Late Archaean and Palaeoproterozoic times the paucity of acceptable poles during this lengthy and remote interval inevitably favours a solution involving differential continental movements (Pesonen et al., 2003). Furthermore, because we are dealing with continental crust likely to be in continuous motion, such an approach based on small polar datasets can only fortuitously hope to configure the continental blocks correctly with respect to one another. However, the quasi-rigid model makes special demands on the data by demanding conformity to a single APW path over a long interval of time. After ~1300 Ma the number of precision poles increases markedly and key recognition of the integrity of Palaeopangaea can be identified in Figs. 2a–4a from the tight conformity of poles with $Q \geq 4$ to a single APW path. As noted below, poles linked to precision age dates also now define a consistent time progression describing APW.

Table 1
Summary of ~1300–500 Ma Palaeomagnetic poles from the major continental shields

Rock unit		Age (Ma)	°N/°E	Reference
North America				
Harp Dykes	1	1273±1	19/228	2056
Seal Group Redbeds	1	1321±190	5/205	2658
Seal Lake Group	1	1321±90	17/195	1604
Mistatin Pluton	1	1317±30	−1/202	2271
Nain Anorthosite	1	1305±15	12/207	2180
NA1	**1**	**1307**	**11/207**	
Coppermine Group	1	1050–1250	1/183	5920
Sudbury Dykes	1	1235±7	−3/192	3496
Muskox Intrusion	1	1270±4	6/191	3484
Mackenzie Dykes	1	1267±2	4/202	5916
Keewatin Mackenzie Dykes	1	1200–1300	3/190	2649
Mackenzie Dykes	1	1267±2	4/193	3187
Mackenzie Dykes	1	1267±2	1/189	2663
Sudbury Dykes	1	1235±7	−3/193	2175
Savage Point Sills	1	1190–1290	−3/183	1747
NA2 (Mackenzie Episode)	**1**	**1267**	**1/190**	
Spokane Formation	1	1200–1400	−16/226	2076
Klinta Formation	1	1100–1400	−7/208	3631
Montagnais Dykes	1	1150–1400	−10/223	2220
NA3	**1**	**1265**	**−11/219**	
Abitibi Dykes	2	1141±2	44/211	7193
Baraga County Dykes	2	1100–1200	49/238	1617
Alona Bay Volcanics	2	1050–1150	47/233	3065
South Trap Range Lavas	2	1050–1150	29/233	3091
Coldwell Complex	2	1108±1	54/217	6493
Logan Sills (N)	2	1108±4	48/218	3056
Powder Mill Volcanics	2	1100–1300	39/218	349
Marquette Dykes	2	1100–1200	48/214	1616
NA4	**2**	**1132**	**45/223**	
Logan Sills (R)	2	1108±4	47/220	3024
Mamainse Point Lavas (R)	2	1084–1100	49/232	3064
Garagantua Volcanics (R)	2	1050–1150	72/223	3061
Gargantua/Mamainse (R)	2	1050±50	50/226	2661
Thunder Bay Dykes (R)	2	1085–1185	48/212	1311
Osler Volcanics (R)	2	1050–1150	49/203	3057
NA5		**1098**	**53/219**	
Aillik Dykes	2	950–1100	27/224	2600
Lackner Lake Carbonatite	2	1092±21	54/204	8381
Nemagosenda Complex	2	1097–1117	51/188	7303
Duluth Gabbro	2	1091±14	48/183	3154
Seabrook Lake Carbonatite	2	1113±36	46/180	6671
Society Cliffs Dolostone	2	1085–1105	43/168	9250
Osler Volcanics	2	1090–1110	43/195	2612
Keweenawan Intrusives	2	1091±41	42/191	3018
Shenango Alkaline Complex	2	1030–1080	39/189	7302
Lackner–Borden Carbonatite	2	1095–1115	39/185	7324
Chipman Lake Carbonatite	2	1050–1150	38/186	6668
Mamainse Point Formation	2	1084–1100	38/186	944

Table 1 (*continued*)

Rock unit		Age (Ma)	°N/°E	Reference
North America				
Mamainse Point Volcanics (N)	2	1114±25	37/180	3063
Thunder Bay Dykes (N)	2	1085–1185	36/175	1310
Mellon Gabbro	2	1077–1105	36/185	3166
NA6		**1099**	**41/184**	
(above 13 results)				
Gila County Dolerite Sills	2	1070–1110	−25/205	7191
Logan Dykes	2	979–1079	35/181	2980
Copper Harbour Lavas	2	1100–1150	35/176	1655
Lester River Sill	2	1054–1084	35/199	3021
Gargantua Volcanics (N)	2	1050–1150	34/180	3060
North Shore Volcanics	2	1115±15	33/183	5900
Duluth Gabbro	2	1091±14	33/199	2617
Cardenas Volcanics	2	1091±5	32/185	9073
Endion Sill	2	1069±15	32/189	3020
Gargantua/Mamainse (N)	2	1050±50	30/183	2660
Michipicoten Point Volcanics	2	1050–1150	29/179	3062
Beaver Bay Complex	2	1077–1105	28/190	3153
Franklin Mountains Rocks	2	1085–1110	28/200	3001
Portage lake Lavas	2	1096±2	27/183	5894
Firesand River Carbonatite	2	1080–1100	27/183	8380
Clay Howells Carbonatite	2	1075±15	27/178	6475
Gila County Diabase	2	1150±30	27/179	2940
Logan Diabase	2	1077–1105	26/194	3023
Michipicoten Island Formation	2	1070–1088	26/175	945
Portage Lake Volcanics	2	1096±2	24/176	5901
Sibley Conglomerate	2	1000–1100	22/184	9082
Lake Shore Traps	2	1087±2	22/181	7198
Isle Royale Lavas	2	1000–1200	21/176	5898
Chengwater Volcanics	2	1050–1115	18/188	8163
NA7	**2**	**1086**	**29/184**	
Jacobsville Formation	2	1000–1100	12/175	2020
Copper Harbour Conglom.	2	1000–1100	11/168	277
Nonesuch Shale	2	1046±46	8/178	2053
Pikes Peak Granite	2	1030–1050	6/181	3041
Freda Sandstone	2	1050–1060	2/179	2051
Rama County Diabase	2	850–1200	1/177	2811
Cardenas Lavas	2	1090±70	0/185	2591
Chequamegon Sandstone	2	950–1050	−12/178	1679
NA8	2	**1046**	**4/178**	
Amnicon and Orienta Formation	2	950–1050	25/148	1642
Steel Mountain Anorthosite	2	900–1100	23/139	2261
Eileen Formation	2	950–1050	20/156	1644
Tudor Gabbro	**2**	1110±20	17/138	2604
Fond du Lac Formation	2	950–1050	16/160	1640
River Valley Anorthosite	2	900–1100	8/161	2605
Sudbury Dyke o/p	2	900–1100	4/163	2173
Uinta Mountain Group	2	900–1000	1/157	683
NA9	2	**1016**	**14/153**	

Table 1 (*continued*)

Rock unit		Age (Ma)	°N/°E	Reference
Grenville Dykes	2	900–1200	−36/175	5839
Haliburton A component	2	1000–1030	−33/142	9165
Morin Anorthosite Complex	2	900–950	−42/141	2475
Gatineau Metamorphic Rocks	2	900–1200	−32/156	2976
Thanet Gabbro	2	1000–1050	−28/158	2181
Lac Allard Anorthosite	2	900–1100	−39/140	3406
Borden Dykes	2	900–1000	−27/153	1686
NA10	**2**	**1002**	**−34/152**	
Grenville Diabases	2	700–1000	−3/151	2989
Chibougamau CH Component	2	900–1000	−7/155	**
Indian Head Anorthosite	2	900–1100	−8/158	2260
Umfraville Gabbro	2	1160–1200	−11/166	2079
Whitestone Anorthosite W_S	2	950–1000	−16/156	**
Wilberforce Pyroxenite	2	800–1100	−14/148	2603
Whitestone Anorthosite Z	2	950–1000	−22/140	2616
Magnetawan Metasediments	2	900–1100	−24/130	5871
NA11	2	**985**	**−13/151**	
Whitestone Anorthosite W_Z	2	850–1000	−16/156	**
Cordova Gabbro	2	850–950	−11/151	130
Nankoweap Formation	2	850–900	−10/163	9074
Kingston Dykes	2	800–900	−12/163	2667
Lac St Jean Anorthosite	2	900–950	−8/167	1684
Haliburton C Component	2	850–1000	−1/165	**
St Urbain Anorthosite	2	900–1000	3/153	5841
Mt Nelson Fm. Goat R. o/p	2	800–900	10/156	1693
NA12	**2**	**900**	**−6/159**	
Galenos Formation	2	780–820	−2/163	9138
Tsezotene Formation	2	780–880	12/146	341
Mudcracked Little Dal	2	780–850	−9/143	1712
Basinal Little Dal	2	780–850	−16/141	244
Rusty Shale Formation	2	780–850	−8/133	6591
Reynolds Point Fm.	2	780–850	−6/147	1700
NA13	**2**	**815**	**−5/146**	
Little Dal Lavas	3	778±2	24/115	1674
Kwagunt Formation	3	736–748	18/166	9137
Redstone Formation	3	730–780	22/151	6597
Natkusiak Formation (i)	3	720–726	6/159	1696
Natkusiak Formation (ii)	3	720–726	−7/163	2628
Rapitan Group	3	650–750	−7/194	2143
Glen Mtns. Layered Complex	3	680–780	−20/200	1213
NA14	**3**	**729**	**2/172**	
(above 6 results)				
Franklin Dykes	3	723±3	9/153	1687
Brock Inlier Sills	3	720–726	−2/165	1660
Aston Bay Dykes	3	720–726	−18/164	2080
Baffin Island Dykes	3	720–726	6/168	2601
Keewatin Franklin Dykes	3	720–726	3/161	2648
Coronation Sills	3	720–726	−1/163	2965
Sanyunei Formation	3	700–750	1/154	8147
NA15	**3**	**723**	**0/161**	
(Franklin Episode)				
Tremblay Sound Dyke	3	650–750	26/166	1688

(continued on next page)

Table 1 (*continued*)

Rock unit		Age (Ma)	°N/°E	Reference
Catoctin Basalts	4	597±18	−42/117	7474
Callander Alkaline Complex	4	575±5	−46/121	6458
Bluewater Formation	4	550–600	−64/110	7773
NA16 (above 3 results)	**4**	**582**	**−51/117**	
Buckingham Volcanics	4	573±32	−9/161	1645
Rainstorm Member	4	542–670	−10/162	164
Unicoi Basalts	4	540–600	0/179	702
Double Mer Formation	4	542–600	−14/176	6938
NA17	**4**	**580**	**−8/170**	
Skinner Cove Basalts	4	550±3	15/157	8321
Tapeats Sandstone	4	501–542	5/158	2193
Wichita Granites	4	525±25	2/147	3317
Bradore Formation	4	513–542	29/167	2256
Waynesboro Formation	4	501–542	28/165	215
NA18	**4**	**530**	**16/158**	
Sept Isles layered Complex	4	565±4	20/141	1752
McClure Mountain Complex	4	535±5	18/142	742
Rome Formation	4	501–542	42/142	216
NA19	**4**	**541**	**27/142**	
Sept Isles Dykes	4	565±4	−44/135	1754
Colorado Dykes	4	497±16	37/102	450
Muav Limestone	4	501–513	55/110	2192
Nolichuky Formation (i)	4	494–501	41/109	697
Colorado Intrusives	4	485–704	48/107	2101
NA20 (above 4 results)	**4**	**523**	**45/107**	
Nolichuky Formation (ii)	4	494–501	39/131	698
Hickory Formation	4	494–501	34/140	210
Cap Mountain Formation	4	494–501	33/140	211
Lion Mountain Member	4	494–501	32/142	212
Bright Angel Shale	4	488–501	30/141	269
Covey Hill Formation	4	488–513	46/149	688
Rocky Mountain Limestones	4	458–505	24/141	687
NA21	**4**	**496**	**34/140**	
Wilberforce Formation	4	488–501	6/159	2245
Morgan Creek Limestone	4	488–501	11/158	6173
Royer Dolomite	4	488–501	13/157	5976
NA22	**4**	**495**	**10/158**	
Taum Sauk Limestone	4	494–501	−4/176	323
Moore Hallow Group	4	488–501	−1/163	6192
Colorado Metaigneous Conts.	4	494–514	−6/169	6172
NA23	**4**	**499**	**−4/169**	
Hebridean Craton, NW Scotland				
Stoer Group, Lower	1	1199±70	26/244	9198
Stoer Group, Middle	1	1199±70	35/241	9199
Stoer Group, Upper	1	1199±70	38/242	9200
HC1	**1**	**1199**	**33/242**	**(33/203)**
Diabaig Formation	2	994±48	−1/234	Piper and Darabi (2005)
Applecross Formation	2	997±39	2/239	Piper and Darabi (2005)
Aultbea Formation	2	997±39	0/235	Piper and Darabi (2005)
Cailleach Head Formation	2	997±39	8/222	Piper and Darabi (2005)
HC2	**2**	**997**	**2/233**	**(2/195)**

Table 1 (*continued*)

Rock unit		Age (Ma)	°N/°E	Reference
Greenland				
Basal Eriksfjord Group Lavas	1	1282–1316	10/207	Piper (1992)
Eriksfjord Gp., Lower Lavas	1	1282–1316	7/239	Thomas and Piper (1992)
Eriksfjord Lavas, Upper Lavas	1	1282–1316	16/222	Thomas and Piper (1992)
Grønnedal–Ika Complex	1	1299±17	9/228	7529
BD0 dykes	1	1250–1299	11/227	2104
GR1 (Early Gardar Episode)		**1294**	**11/229**	**(15/213)**
North Qôroq Complex	1	1268±60	14/201	6607
Narssassuaq Stock	1	1160–1290	9/207	6606
BD0 Dyke	1	1284±3	−12/203	Piper (1995)
Motzfeldt Complex	1	1282±1	10/212	Piper (1992)
Lamprophyre Dykes	1	1250±18	3/206	2108
BD1 Dykes, western sector	1	1200–1270	4/208	Piper (1995)
BD1 Dykes, north-west sector	1	1200–1270	3/215	7628
Post Grønnedal Dykes	1	1200–1270	7/220	Piper (1994)
W. Greenland kimberlite suite	1	1227±12	3/215	839
Kûngnât Fjeld Complex	1	1219±16	3/199	2107
GR2	**1**	**1247**	**4/209**	**(9/192)**
Zig Zag Dal Basalts	1	1200–1300	12/243	98
Midsommersoe Dolerite	1	1250±50	7/242	99
Victoria Fjord Dolerite dykes	1	1250±50	10/232	489
GR3 (N. Greenland Episode)		**1250**	**10/239**	
BD2–BD3 Dykes, W. sector	1	1227±29	30/220	Piper (1995)
BD2–BD3 Dykes, NW sector	1	1227–1270	40/227	Piper (1995)
BD2–BD3 overprints in Unit 1	1	1227–1270	25/229	Piper (1995)
Hviddal Giant Dyke, Tugtutôq	1	1184±5	33/215	2132
Narssaq Gabbro	1	1107–1179	32/225	2133
Younger Giant Dykes	1	1143±36	42/226	2131
BD3 Dykes, eastern sector	1	1143–1160	36/224	2105
BD3 Dyke swarms, NW sector	1	1143–1160	33/231	6609
South Qôroq Complex	1	1160±8	42/214	6610
GR4 (Mid-Gardar episode)	**1**	**1184**	**35/224**	**(40/210)**
Ilímaussaq Complex	**1/ GR5**	**1143±21**	73/282	8454
Eriksfjord Group, Gardar o/p	1	1100–1143	48/244	Piper et al. (1999)
Fennoscandian Shield (Baltica)				
Dala Sandstones	1–1	1250–1500	33/177	1324
Sub-Jotnian Lavas	1–1	1250–1500	27/189	1325
Ragunda Formation	1–1	1293±30	52/167	1320
Ragunda Rapakivi Suite	1–1	1293±30	49/171	5788
FS1	1–1	**1334**	**41/177**	**(33/222)**
Market Dolerites	1–1	1265±6	−6/146	3093
Fennoscandian Shield (Baltica)				

Table 1 (*continued*)

Rock unit		Age (Ma)	°N/°E	Reference
Vaasa Dolerites	1–1	1225–1270	7/164	3460
Satakunta Dolerites	1–1	1200–1350	2/158	3478
Sarna Dolerites	1–1	1215–1290	5/159	1326
Storsjon–Edsbyn Sills	1–1	1240–1310	12/162	8685
Vigehavn and Bolshavn Dykes	1–1	1100–1400	14/156	2136
FS2	1–1	**1256**	**6/158**	**(18/181)**
Post-Ragunda Dykes	1–1	1250–1320	15/194	1321
Kjeldsea Dyke	1–1	1000–1400	7/179	5792
FS3	1–1	**1243**	**11/186**	**(5/207)**
Vasterbotten Complex	1–1	1240–1310	−8/158	8686
Ulfo Complex	1–1	1240–1310	−8/157	8687
Jamtland Complex	1–1	1240–1310	1/161	8688
Satakunta Complex	1–1	1240–1310	−2/162	8689
Nordingra Basic Dykes 2	1–1	1200–1300	5/168	5796
Ulvo Dolerite Dykes	1–1	1215±20	1/161	5798
Gavle Dolerite	1–1	1200–1300	7/150	2298
Nordingra Dolerite	1–1	1245±20	−5/158	2299
Jotnian Dolerites	1–1	1245±20	0/155	2300
Alvdelsassen Dolerite Sill	1–1	1231±18	1/149	935
Ulvo Dolerites	1–1	1215±20	1/161	5798
Gnarp Sills	1–1	1213–1270	−13/146	5795
Vaster–Norrland Dolerites	1–1	1213–1270	−8/157	5
Bornholm Group B Dykes	1–1	1150–1250	0/155	7639
Giman Dolerite	1–1	1179–1229	−5/152	5800
FS4 (Jotnian Episode)		**1243**	**−3/156**	**(12/174)**
Laanila Dykes	2	998±80	−4/218	5744
Laanila–Ristijarvi Dykes	2	1042±50	−2/212	8275
FS5	**2**	**1020**	**−3/215**	**(7/149)**
Kautokeino Dykes	2	1066±34	−36/236	8276
Bamble Terrane V	2	920–900	−47/250	Piper (in press)
Telemark Terrane III	2	920–900	−33/243	Piper (in press)
Rogaland Farsundite	2	977±36	−44/232	894
Rogaland Migmatites	2	901–953	−50/244	5808
FS6	**2**	**976**	**−41/241**	**(−31/172)**
Egersund Dykes	2	842–945	−25/232	3007/3635
Bamble Terrane IV	2	920–900	−27/234	Piper (in press)
FS7	**2**	**962**	**−26/233**	**(−16/166)**
Scania Intrusions	2	750–1050	−49/211	1330
W. Sweden Minor Dykes	2	900–1100	−46/223	910
Haaland–Helleren Massif	2	977±36	−41/213	899
Bjerkrem–Sogndal Lopolith	2	945±40	−41/217	900
Alvesta–Ljungby Group I	2	940–960	−43/221	8256
Garsaknett Leucorite	2	902±30	−40/221	897
Hidra Leuconorite	2	872–932	−43/220	896
W. Sweden minor Dykes	2	850–950	−46/223	910
Hunnendalen Dykes	2	855±59	−41/222	8299
FS8	**2**	**926**	**−43/219**	**(−33/153)**
Aana–Sira Massif	2	928–902	−46/197	898
Egersund Farsundite	2	928–902	−43/194	2295
Egersund Anorthosite	2	890–910	−42/200	5810
Rogaland Basement rocks	2	842–945	−36/207	3005
Karlshamn Dolerite Dyke	2	954±1	−40/210	2757/5805
FS9	**2**	**915**	**−42/201**	**(−32/137)**

Table 1 (*continued*)

Rock unit		Age (Ma)	°N/°E	Reference
Bamble–Kongsberg Amphibolites	2	920–850	−8/208	2756
Alvestsa–Ljungby Group III	2	900–1000	−12/211	8259
Telemark Terrane II	2	920–850	−16/214	Piper (in press)
Bamble Terrane III	2	920–850	−16/200	Piper (in press)
Bamble Intrusions	2	920–850	6/200	904
FS10	**2**	**898**	**−9/207**	**(1/141)**
Bamble Terrane II	2	920–850	9/228	Piper (in press)
Dolerites E. of Protogine Zone	2	870–995	8/243	2187
Bratton and Algon Intrusions	2	920–850	5/249	909
Alvesta–Ljungby Group II	2	850–950	−9/239	8258
Alvesta–Ljungby Group IV	2	850–950	1/244	8260
Blekinge–Dalarna Dolerites	2	844–935	10/241	6528
Listed Dyke	2	800–1000	14/250	2134
FS11	**3**	**899**	**5/242**	**(14/177)**
Telemark Terrane I	2	900–800	−2/256	Piper (in press)
Bamble Terrane I	2	900–800	2/266	Piper (in press)
Kanna Gneiss LBT comp.	2		21/256	Pisarevsky and Bylund (1998)
Rogaland Y Component	2		−7/236	Stearn and Piper (1984)
FS12	**3**	**850**	**2/253**	**(10/188)**
Kildinsk Series, Kola	3	700–750	20/197	5628
Oje Basalts	3	745–931	32/185	5774
Vadso and Barents Sea Groups	3	700–800	23/209	7536
FS13	**3**	**771**	**25/197**	**(35/129)**
Batsfjord Dykes	3	610–670	−41/287	2312
Nyborg Formation	3	653±7	−24/269	7740
FS14	**3**	**646**	**−16/277**	**(−17/200)**
Sarv Nappe Dolerites	3	615–715	−21/350	1327
Fen Tinguaites	4	583±15	−50/324	621
Fen Carbonatite	4	583±15	−56/330	8764
FS15 (2 above results)	**4**	**583**	**−53/327**	**(−55/247)**
Kildinsk Series, Kola	4	542–600	−50/264	5618
Winter Coast Sediments	4	555±3	25/312	8923
Alnon Complex	4	545–589	7/272	1328
Nekso Sandstone (i)	4	513–542	−38/315	1988
Nekso Sandstone (ii)	4	513–542	−40/357	9173
Tornetrask Formation	4	530–545	−56/296	8707
N. Norway Intrusions	4	490–530	−31/266	6135
Ukrainian Shield				
Avzyan Group I	1	1263–1350	36/173	5554
Avzyan Group II	1	1100–1350	36/177	5543
Avzyan Group III	1	1150–1250	36/173	5553
Ukraine Intrusives	1	1000–1320	27/194	5679
UK1	**1**	**1223**	**34/180**	**(26/218)**
Rafalivka Lavas	4	551±4	36/333	9125
Bazaltovoe Lavas	4	551±4	26/286	9126
Siberia				
Okhotsky Massif Sediments	1	1050–1350	75/157	6844
Dorbinskaya Suite	1	1050–1350	7/100	6876
Arymassk Group	2	1200–1260	−12/70	5656
Unguokhtakh Group	2	1050–1350	−23/75	5654
Linok Formation	2	1035–1100	15/76	8572

(continued on next page)

Table 1 (*continued*)

Rock unit		Age (Ma)	°N/°E	Reference
Siberia				
Balagannakh River sediments	2	1070–1170	−6/74	5655
Malgina Formation	2	1004–1150	25/51	8571
S1 (above 5 results)	**2**	**1141**	**0/69**	**(10/153)**
Linok Suite	2	980–1100	15/74	7992
Derevninskaya Suite	2	980–1100	20/73	7989
Lena River Igneous Rocks	2	800–1000	5/51	5688
Udjinsk Group	2	800–1000	−6/59	5650
Sukhotungusinskaya Suite	2	980–1100	8/45	7990
S2	**2**	**984**	**9/60**	**(23/149)**
Turukhansk Sediments	2	980–1100	3/148	7987
Slyudyankinskaya Suite	2	819–900	−5/152	7353
Kandykskaya Suite	2	950–1000	−3/177	8935
Ust–Kirbinskaya Suite	2	930–970	−8/183	8936
Anabar Shield Dolerites	2	820–1135	10/203	5576
Lena River Redbeds	3	580–650	−3/168	8473
Mamakanskaya Suite	4	542–600	12/21	7908
Lena River Volcanics	4	542–600	−7/48	5672
Shaman Formation	4	542–600	−32/71	8694
Nokhtuskaya Suite	4	542–600	−31/71	7909
Tagul River Redbeds	4	542–600	−56/110	5561
Kholodninskaya Suite (i)	4	542–600	−28/133	7907
Kholodninskaya Suite (ii)	4	542–600	25/132	7912
Kessyusa Formation	4	535–542	−38/165	8224
Emyaksa Group	4	522–542	−39/153	5428
Pestotsvetna Group	4	522–542	−46/181	5429
Lena River Sediments	4	513–542	17/245	1131
Erkekat Formation	4	513–535	−45/156	8225
Udzha River Sediments	4	513–542	−32/137	5471
Khorbusvonka Toyonian Seds	4	513–525	−46/137	8978
Olenek River Sediments (i)	4	501–513	−31/141	5448
Olenek River Sediments (ii)	4	505–511	−36/135	5469
Yunkyulyabit Formation	4	501–513	−36/140	8226
S3 (above 6 results)	**4**	**517**	**−38/141**	**(−59/192)**
South America Cratons and bordering mobile belts				
Nova Floresta Formation	**1/ SA1**	1199±5	−25/345	8827
Olivenca Dykes-R	2	1078±18	10/280	6324
Itaju do Colonia	2	1012–1078	−8/291	6326
Olivenca Dykes-N	2	1012–1078	−16/287	6325
Ilheus Dykes	2	1012±24	−30/280	6323
SA2 (above 4 results)	**2**	**1045**	**−11/285**	**(35/175)**
La Tinta Formation	**3/ SA3**	709±24	−79/301	63
Campo-Alegre Formation	4	595±5	−57/223	493
Pan de Azucar Formation	4	540–560	−18/251	8930
Puga Cap Carbonate	4	560–600	−83/293	9247
Castro Group Rhyolites	4	520–600	−76/4	495
Acampamento Velho Fm.	4	510–553	−61/338	496
Cerro Totora Formation	4	518–545	37/314	8330
Juiz de For a Complex	4	500–535	4/320	9232
Sierra de las Animas	4	501–520	6/338	8929
Choschas Volcanics	4	502±10	58/309	7564
Hilario Formation	4	492–512	−14/48	499
Indian Shield				

Table 1 (*continued*)

Rock unit		Age (Ma)	°N/°E	Reference
NDII Dyke	1–1	1206±2	−46/30	Goutam et al., submitted for publication
Kaimur Series	1–1	1100–1200	−82/106	3467
Oddanchatram Anorthosite	2–1	1000–1100	−10/182	9150
Wajrakarur Kimberlite	2–1	1050–1100	−46/239	7551
ID Dykes	2	936±1	6/336	Goutam et al., submitted for publication
RD Dykes	2	929–813	−72/97	Goutam et al., submitted for publication
Harohalli Dykes	2/3	808–837	−27/257	8142
Malani Igneous Suite	3	771±2	−68/268	8690
Malani Rhyolites	3	730±10	−78/225	3585
IND1 (above 2 results)	**3**	**751**	**−74/253**	**(2/141)**
Bander and Rewa Series	4	530–650	−47/33	2048
Jutana Formation	4	507–525	−21/51	574
Salt Pseudomorph Beds	4	505–518	−27/34	2716
IND2 (above 3 results)		**539**	**−32/40**	**(−5/213)**
Seychelles				
Mahe Granites	3	755±1	54/38	7555
Mahe Dykes	3	750±3	55/58	8693
SY1	**3**	**753**	**55/48**	**(6/142)**
Madagascar				
Stratoid granite overprint	4	521±12	9/168	8953
Carion Granite	4	532±5	7/181	8673
MG1	**4**	**527**	**8/175**	**(−9/209)**
East Antarctica				
Coats Land Nunataks	**2/ ANT1**	1112±4	23/80	8235 **(56 220)**
Vestfjold Hills Dykes+	2	1010±200	17/193	2673
Zanuck Granite	4	521±2	−7/36	8468
Liberty Hills Formation	4	490–520	7/326	8553
Mirnyy Charnockites	4	520±24	2/28	2715
Wright Valley Granites	4	500±43	5/199	1077
Arabian Peninsula				
Timna Igneous Complex*	4	610–630	84/223	7462
Arfan and Juqjuq Fm.	4	590–620	77/298	1196
Mirbat Sandstone	4	530–560	−23/322	8489
Jordan Dykes	4	513–542	−26/341	1191
Diorite Stock	4	501–542	26/332	1197
Africa, Kalahari Craton				
Barby Formation Lavas	1	1190±38	68/28	2566
Premier Kimberlite	1	1120–1220	51/38	3288
K1		**1179**	**55/46**	**(51/217)**
Kimberlite pipes	2	1124–1223	34/55	7545/7546
Umkondo Lavas	2	1105±2	63/16	3425
Umkondo Dolerites	2	1105±2	65/40	3447
Timbavati Gabbros	2	1103–1107	63/47	8140
Post-Waterberg Dolerites	2	1091±15	65/51	3437
K2 (4 above results)	**2**	**1102**	**65/39**	**(53/200)**
Kalkpunt Formation	2	800–1050	57/3	891
Guperas Lavas	2	1020–1150	63/317	2567
Auborus Formation	2	800–1020	43/354	2568
K3	**2**	**1040**	**56/352**	**(31/187)**

Table 1 (*continued*)

Rock unit		Age (Ma)	°N/°E	Reference
Port Edward Pluton	2	1017–1033	−7/328	9135
Africa, Kalahari Craton				
Ntimbankulu Pluton	2	1000–1100	27/327	8611
O'okiep intrusions	2	1020±30	15/335	2565
Namaqualand Metamorphics	2	980–1020	8/330	1566
K4	**2**	**1024**	**11/330**	**(−17/186)**
Lower Nama Group	4	600–700	61/63	1254
Nama Group Sediments	4	510–570	73/48	8219
Upper Nama Group	4	550–600	5/271	1256
Sijarira Group	4	500–700	2/352	3211
Equeefa Dykes	4	510–550	24/17	9134
Ntonya Ring Structure	4	522±13	28/345	3353
K5 (above 3 results)		**551**	**14/358**	(−4/211)
Africa, Damaran Belt				
Nosib Group	2	840–1080	28/323	247
Mulden Group	4	555±5	13/270	252
Doornpoort, Damaran o/p	4	500–550	−22/245	2562
Africa, Tanzanian Craton				
Post-Kibaran intrusives	**1**	1236±24	17/293	8123
Ikorongo Group	**2**	850–1000	35/264	2911
Kigonero Flags	2	750–850	12/273	2503
Bukoban Dolerites	2	806±30	−11/281	2500
Mbala Dolerites	2	776–836	−2/278	2905
Gagwe Lavas	2	795±7	−25/273	7785
T1 (above 3 results)	**2**	**836**	**2/274**	**(−27/216)**
Mbozi Complex	3/**T2**	743±30	46/325	7786
Sinyai Metadolerite	4	547±4	−29/139	8126
Africa, Pan African Belts				
Suakin Gabbro	2	841±4	−25/314	7760
Barramiya Chromite*	4	670–900	74/113	6219
Dokhan Volcanic Fm. (i)	4	580–611	−36/17	199
Dokhan Volcanic Fm. (ii)	4	570–610	43/216	8118
Nabati Complex	4	569–587	68/314	1181
Bir Safsaf Dykes	4	573–599	80/250	1182
Abu Durba Sediments (i)	4	513–542	18/341	7221
Abu Durba Sediments (ii)	4	488–542	−30/56	7222
Esh El Mellaha Dykes	4	488–542	87/26	8115
Um Rus Dykes	4	486–497	85/166	201
Qena–Safaga Dykes	4	480–527	87/304	198
West Africa Craton				
Group de Char I2	2–1/**WA1**	1019±32	54/32	2178
Char Group Unit I2	2–1	966–1030	49/207	378
Atar Group Unit I9	3–1	775±52	34/247	379
Adma Diorite	3–1	613±3	34/344	69
Bou Azzer–El Graara Sediments	4–2	512–548	47/42	2123/2184
Sidi Said Maachou Volcanics	4–2	501–513	14/235	7626
Atar Cliff, CO7 and 8	4–2	488–542	0/249	380
WA2 (above 2 results)	**4**	**511**	**7/240**	**(−37/105)**
Australia				
Mt. Barren Metasediments	(a)	1205±10	47/347	8981
Bremer Bay Metamorphics	(a)	1100–1200	74/304	8980
AU1	**(a)**	**1189**	**60/332**	**(−5/216)**
Lake View Dolerite	(b)	1120±10	12/304	1928
Mt Isa IAR Dykes	(b)	1116±12	10/311	7549

Table 1 (*continued*)

Rock unit		Age (Ma)	°N/°E	Reference
AU2	**(b)**	**1118**	**11/308**	**(49/104)**
Australia				
Bangemall Sills	(b)	1171±8	−34/275	8781
Kulgera Dyke Swarm	2–1	1054±14	−17/264	6371
Wooltana Volcanics	2–1	780–883	−62/142	1156
Mundine Dykes	3	755±3	−44/314	8560
Northampton Dykes	3	752–758	−47/317	1155
AU3 (above 2 results)	**3**	**755**	**−46/315**	**(1/170)**
Cap Dolomite/ Walsh Tillite	3	700–800	−22/282	8562
Copley Quartzite	3	750–850	−36/10	1159
Merinjina Tillite	3	750–850	−45/346	1160
Angepena Formation	3	620–650	−33/344	1164
Yaltipena Formation	3	630–620	−44/353	8514
Elatina Formation (i)	3	620–600	−39/2	8515
Elatina Formation (ii)	3	620–600	−52/347	7597
Elatina formation (iii)	3	620–600	−54/327	6354
Elatina formation (iv)	3	620–600	−51/337	560
Brachina formation	3	580–610	−33/328	1168
AU4 (above 6 results)	**3**	**611**	**−46/343**	**(−14/199)**
Lower Arumbera	4	545–560	−44/342	1956
U. Arumbera Sandstone	4	530–560	−46/337	1958
Todd River Dolomite	4	513–542	−43/340	1959
Albany Belt Dykes	4	520–600	−38/347	7585
Antrim Plateau Volcanics	4	520±9	−9/340	1896
AU5	4	**546**	**−36/341**	**(−4/196)**
Bunyeroo Formation	4	593±32	−18/16	8114
Hawker Group A	4	528–542	−21/15	1402
Kangaroo Is. Sediments	4	513–525	−34/15	1405
Billy Creek–Aroona	4	506–528	−37/20	1403
Lake Frome A	4	501–513	−31/27	1401
Giles Creek Dolomite	4	501–513	−38/25	1410
Pertaoorta Group	4	501–542	−33/12	1407
AU6 (above 6 results)	**4**	**518**	**−32/19**	**(−3/228)**
U. Lake Frome sediments	4	488–501	−16/25	1919
South China				
Shicaohe Formation	2	910–1010	−27/39	957*
Songziyan Formation	2	900–1000	−81/300	956*
Macaoyan Group	2	793–893	−6/346	954*
Xiaofeng Dyke swarm	**3/SC1**	**802±10**	**−14/271**	9117
Liantuo Formation	3	748±12	−3/344	8543
Nantuo Formation	3	599–663	−4/341	8149/8545
Doushantouo Formation	4	599±4	−38/35	948*
Doushantouo Carbonates	4	542–603	−1/17	9123
Shuijingtuo Formation	4	513–542	−32/0	1034
Meishucun Formation	4	513–542	9/31	1035
Tianheban Formation	4	513–542	−7/10	1032
Hetang Formation	4	513–542	−3/16	1033
SC2 (above 3 results)	**4**	**528**	**−0/19**	**(48/122)**
N. Sichuan Sediments	4	501–513	51/346	9118
S. China sediments	4	488–542	40/5	9798
SC3		**511**	**46/356**	**(−19/246)**
North China				
Wumishan Formation	1–1	1220–1400	−4/206	974*
Yangzhuang Formation	1–1	1250–1435	−17/240	975*
Basic Intrusives	1–1	1100–1300	−1/211	Zhang et al. (1991)
NC1	**1–1**	**1250**	**−8/219**	**(26/202)**
Sanjiaotang Formation	1–1	800–1000	36/224	8812
Cuizhuang Formation	2	800–1000	47/218	8813*

(continued on next page)

Table 1 (*continued*)

Rock unit		Age (Ma)	°N/°E	Reference
Chang–Longshan Formation	2	805–905	60/243	970
North China				
NC2 (above 3 results)		**885**	**48/227**	**(−1/252)**
Nanfen Formation	2	800–900	−17/121	Liu et al. (1984)
Liulaobei Formation	2	800–900	43/150	Piper and Zhang (1997)
Qiaotou Formation 1	2	750–850	34/177	Zhang (1995)
Nanfen Formation	3	757–837	64/162	966*
Ganzingzi Formation	3	650–750	66/169	962*
Diayutai Formation	3	768–868	61/239	967*
Nangualing Formation	3	650–750	60/219	963*
Dongjia Formation	3	617–683	61/277	8811
Fengtai Formation	4	545–600	62/233	Piper and Zhang (1997)
Houjiasah/Yutaishan Fm	4	545–600	63/234	Piper and Zhang (1997)
NC3 (above 2 results)	**4**	**575**	**63/234**	**(−3/237)**
L. Cambrian Limestone	4	513–542	−19/162	8428
M. Cambrian Sediments	4	501–513	−37/147	8427
Cambrian Sediments	4	501–542	−21/155	6245
U. Cambrian Limestone	4	488–501	−32/150	8426
Zhushadong/Xinji Fms.	4	488–542	−42/149	8810
NC4 (above 4 results)	**4**	**510**	**−33/150**	**(−58/195)**

Numbers in 1 to 4 in column 2 refer to time windows plotted in Figs. 4 to 5. Boldface positions in brackets are pole positions rotated into a Laurentian reference frame. **Pole position included in regional "chrontour" assessment of McWilliams and Dunlop (1978) (a) Poles from Albany–Fraser mobile Belt. (b) Poles from Mt Isa Mobile Belt.

The wider dataset can also be evaluated in the context of the model emerging from the precision data because contoured distributions of rotated poles are able to indicate whether the continental crust was quasi-rigid or undergoing multiple diverse motions (Piper, 1990). Although distributions of the overall data yield less definitive conclusions, they do suggest that the Precambrian database is remarkably robust (Figs. 2b–4b) and minimal criteria work well provided that the palaeogeographic model is appropriate. The contoured distributions of poles are also helpful in contrasting the quasi-integrity of continental crust prior to the continental break-up event in Late Neoproterozoic times with the dispersal of the crust after this event (Bond et al., 1984 and Figs. 5–7).

The probable form of APW during much of Precambrian time appears to be a succession of loops separated by hairpins (e.g. Irving and McGylnn, 1976). The geodynamic significance of this signature has yet to be satisfactorily resolved and analysis is beyond the scope of this paper. Since the APW is evidently applicable to a large continental cap it is likely to be the signature of true polar wander (TPW) resulting from density heterogeneities within the mantle. These rise or fall by buoyancy to perturb the non-hydrostatic inertia tensor of the Earth and cause the tectosphere to migrate with respect to the spin axis until the maximum principal inertia axis (I_{max}) is realigned with the spin axis to force positive mass anomalies towards the equator. Density perturbations in the mantle or core can also potentially cause the Earth's principal inertia axes to interchange: when the maximum principal inertia axis (I_{max}) becomes less than the intermediate axis (I_{int}) the entire silicate Earth can rotate over the liquid outer core by ~90° about I_{min} to align the new I_{max} with the spin axis. This is referred to as Inertial Interchange True Polar Wander (IITPW) and if interchange between I_{max} and I_{int} is merely transient the situation could potentially become highly unstable and produce successive rotations in the opposite sense expressed in the palaeomagnetic record as a ~90° APW loop (Kirschvink et al., 1997; Evans, 1998; Li et al., 2004). The present day viscosity structure of the Earth suggests that IITPW should take no more than 10–20 Myr (Steinberger and O'Connell, 2002). In contrast the Proterozoic APW tracks, although of the order of 90° in length (Figs. 2–4), occupied much longer time intervals of the order of 100 Myr suggesting either that the structure of the Proterozoic mantle was radically different from the present day or that the IITPW mechanism is not relevant here.

The pole positions are plotted on Figs. 2a–5a following rotations according to the Eulerian operations listed in Table 2. The intervals examined are ~1300–1140 Ma, ~1140–800 Ma, ~800–600 Ma and ~600–500 Ma and are selected to illustrate the Gardar Track (Fig. 2), the Keweenawan Track and Grenville–Sveconorwegian Loop (Fig. 3), the Franklin–Adelaide Track (Fig. 4), and continental break-up shortly before the beginning of Cambrian times (Fig. 5). In each case figure (a) shows key anchor poles with ages, and mean poles of Table 1 whilst figure (b) shows all the accepted poles assigned to the interval in question. The assignment of pole positions to Figs. 2–5 is listed as 1 to 4 in the second column of Table 1.

Earlier analyses of Palaeopangaea have suggested that relative movements occurred to achieve peripheral reorganisation of the continental shields at ~1100 Ma during or shortly after the time of Grenville orogenesis (Piper, 1982, 1987, 2000 and Fig. 1). Poles from these peripheral blocks are referred to 'primitive' rotational parameters (Table 2) and coded in the second column of Table 1 as '1–1' etc. The core of the reconstruction comprising Laurentia, central and southern Africa and probably Siberia does not seem to have been perceptibly influenced by this reorganisation and the rotational parameters remain invariant. The primitive positions of Australia, India and south-central Africa follow closely those used hitherto and preserve the close proximity of the Late Archaean–Early Proterozoic nuclei as defined by geological (Rogers, 1996) and palaeomagnetic (Piper, 2003) evidence. The central-southern Africa division comprises the Kaapvaal, Zimbabwe and Tanzania cratonic nuclei with an integral tectonic framework on a palaeomagnetically-detectable scale assumed here to be in place following Kibaran–Irumide orogeny at ~1300–1100 Ma (Fig. 3). Australia comprises the cratonic elements of Western Australia (Pilbara and Yilgan cratons with adjoining King Leopold and Ophalmian mobile belts of Lower Proterozoic age). The South American shield is poorly represented by palaeomagnetic data during the time interval considered here (Table 1). Several views of cratonic relationships have been advocated (e.g. Pimental et al., 1999; Alkmin et al., 2001) and links with the cratons of western Africa evaluated (Trompette, 1997). Most authors consider that the Sao

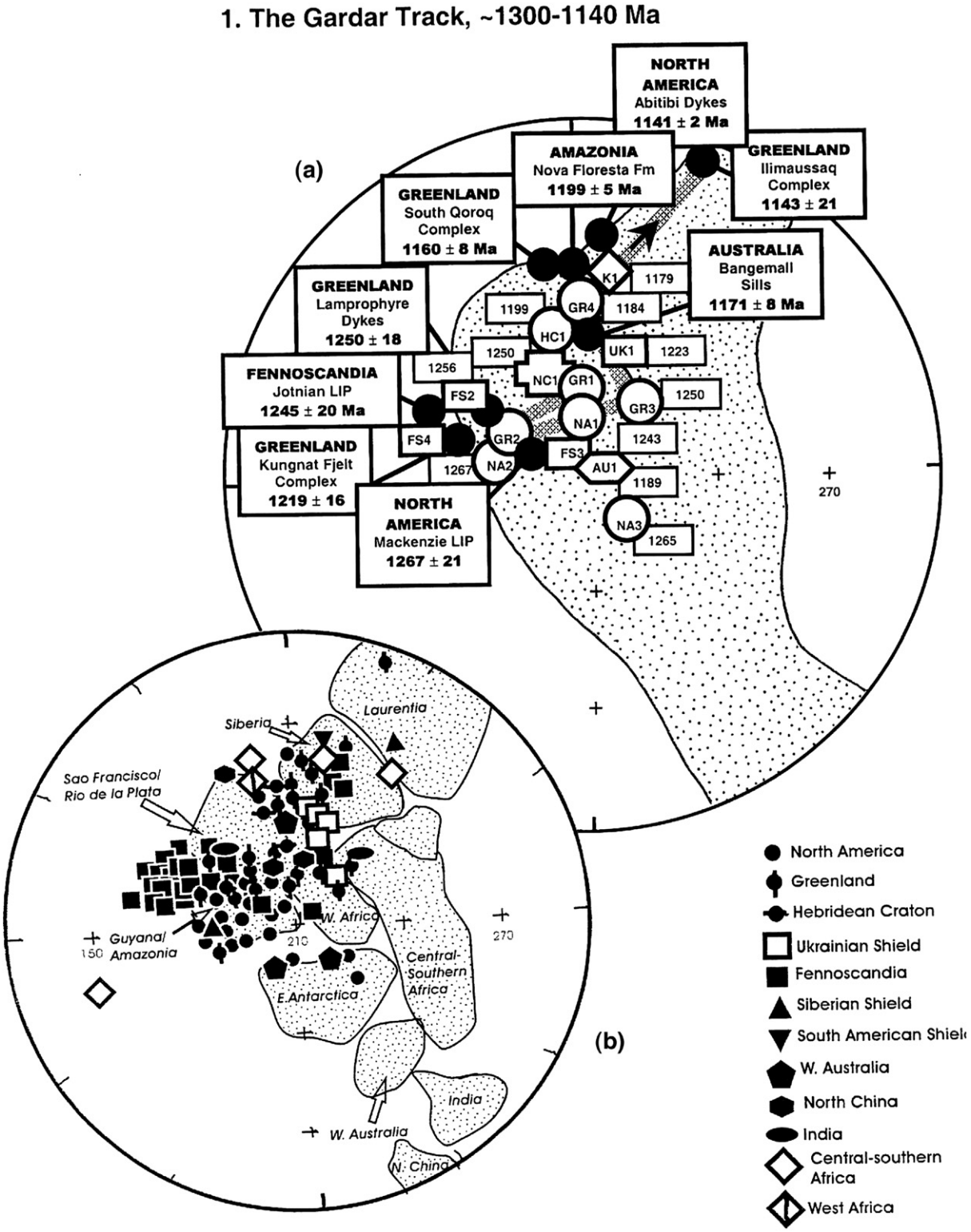


Fig. 2. (a) Summary of anchor poles and mean palaeomagnetic poles (Table 1) assigned to the interval 1300–1140 Ma rotated into a Laurentian reference frame according to Palaeopangaean parameters. The bulk of APW in this interval is assigned to a SW → NE trending (Gardar) palaeomagnetic track. (b) Individual palaeomagnetic poles assigned to this interval (Table 1) rotated into the Laurentian reference frame according to Eulerian parameters listed in Table 2. The area of continental crust is stippled.

Francisco and Rio de la Plata cratons have separate origins and were fused into Gondwana during the Neoproterozoic but a single pole from the latter does not permit this to be tested. For the purposes of the present analysis two divisions are considered, namely Guyana–Amazonia and Sao Francisco–Rio de la Plata (Table 2), acknowledging their contrasting

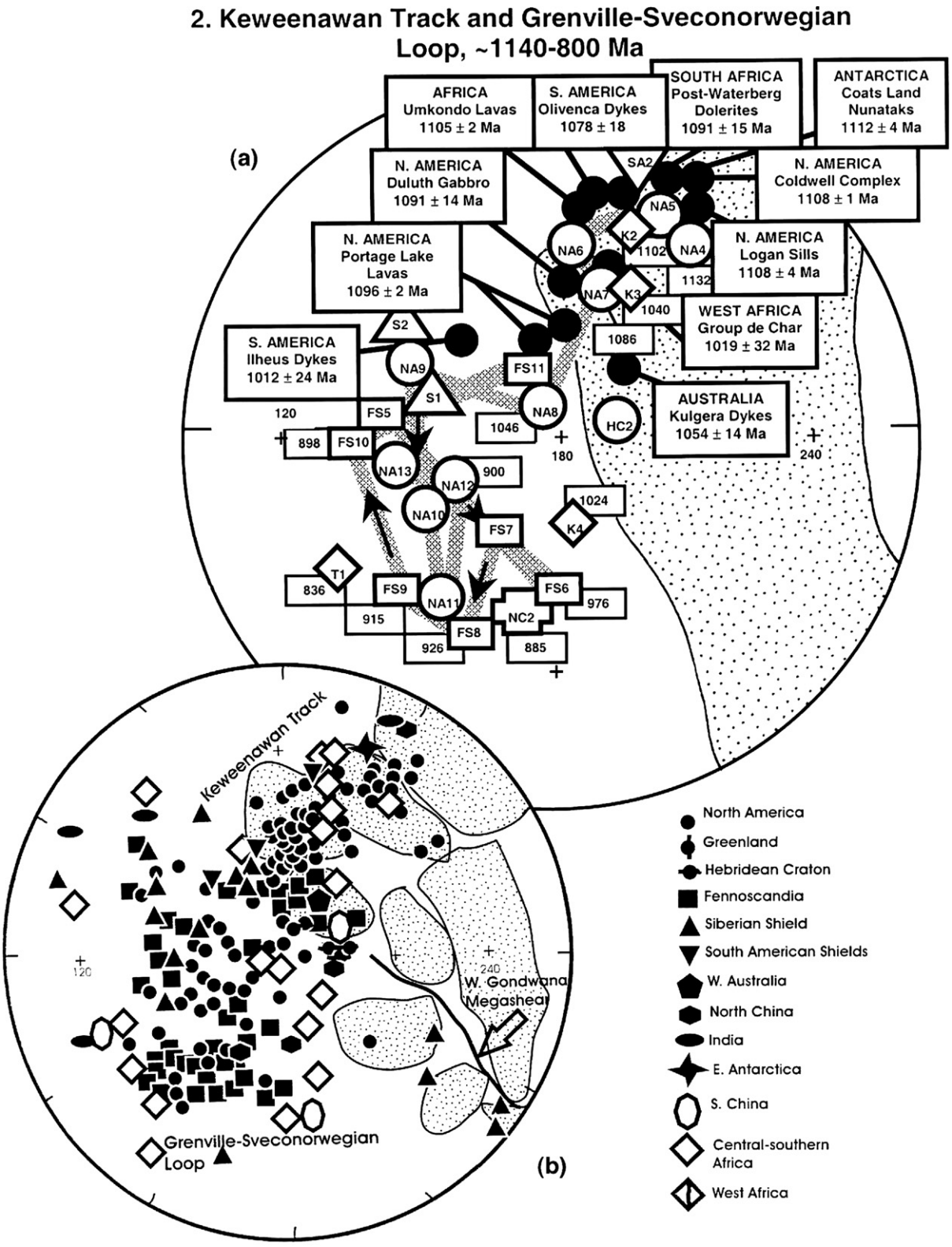


Fig. 3. (a) Summary of anchor pole and mean palaeomagnetic poles assigned to the interval 1140–800 Ma rotated into a Laurentian reference frame according to Palaeopangaean parameters. The bulk of APW in this interval is assigned to a NE → SW trending (Keweenawan) palaeomagnetic track followed by the Grenville–Sveconorwegian loop. (b) Individual poles assigned to this time window (Table 1). The area of continental crust is stippled.

geological histories and the possibility that they were united in subsequent times by large scale strike slip (Onstott and Hargraves, 1981). There are too few data to derive definitive locations for these shields but the configurations of Table 2 show that alternative positions to the west of Africa can overcome the problems with the Rodinia assumption which

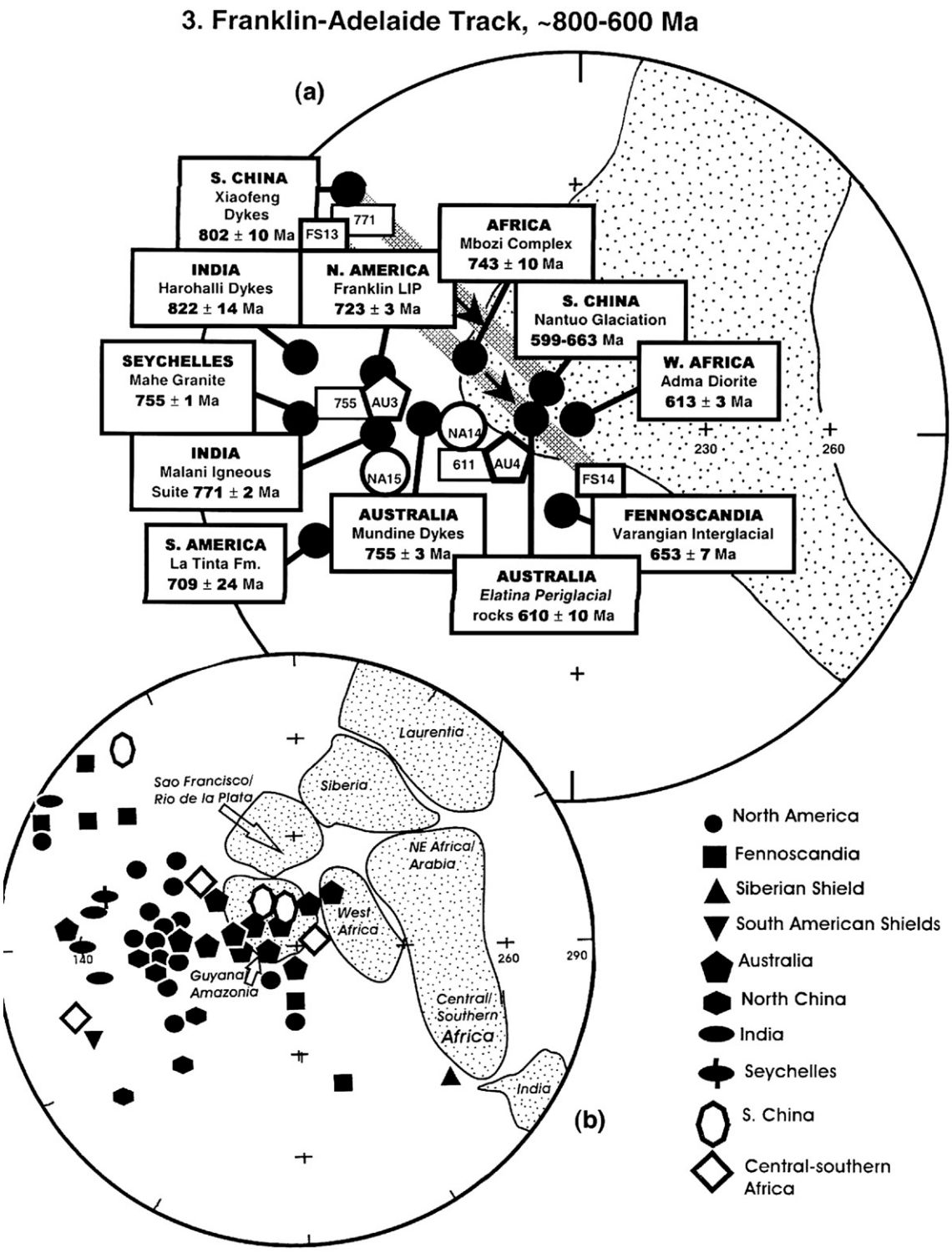


Fig. 4. (a) Summary of anchor poles and mean palaeomagnetic poles assigned to the interval 800–600 Ma rotated into a Laurentian reference frame according to Palaeopangaean parameters. (b) Individual poles assigned to this time window (Table 1). The area of continental crust is stippled.

both acknowledge the links with West Africa and satisfy the palaeomagnetic poles. Although the West African Shield has previously been included with central and southern Africa in present day coordinates (Piper, 1982), this is clearly unsatisfactory in view of their Pan African suture linkage following Dahomeyide and Pharusian orogenesis (Rogers and Santosh, 2004). A relative position southward of its present location achieves a closer match of West African pole WA1 and the dextral transpression required to achieve the Gondwana configuration could then have possibly been accommodated by Pan African dextral shear along the Borborema–Cameroun Belt (Hoffman, 1991). The Palaeopangaean positions of the

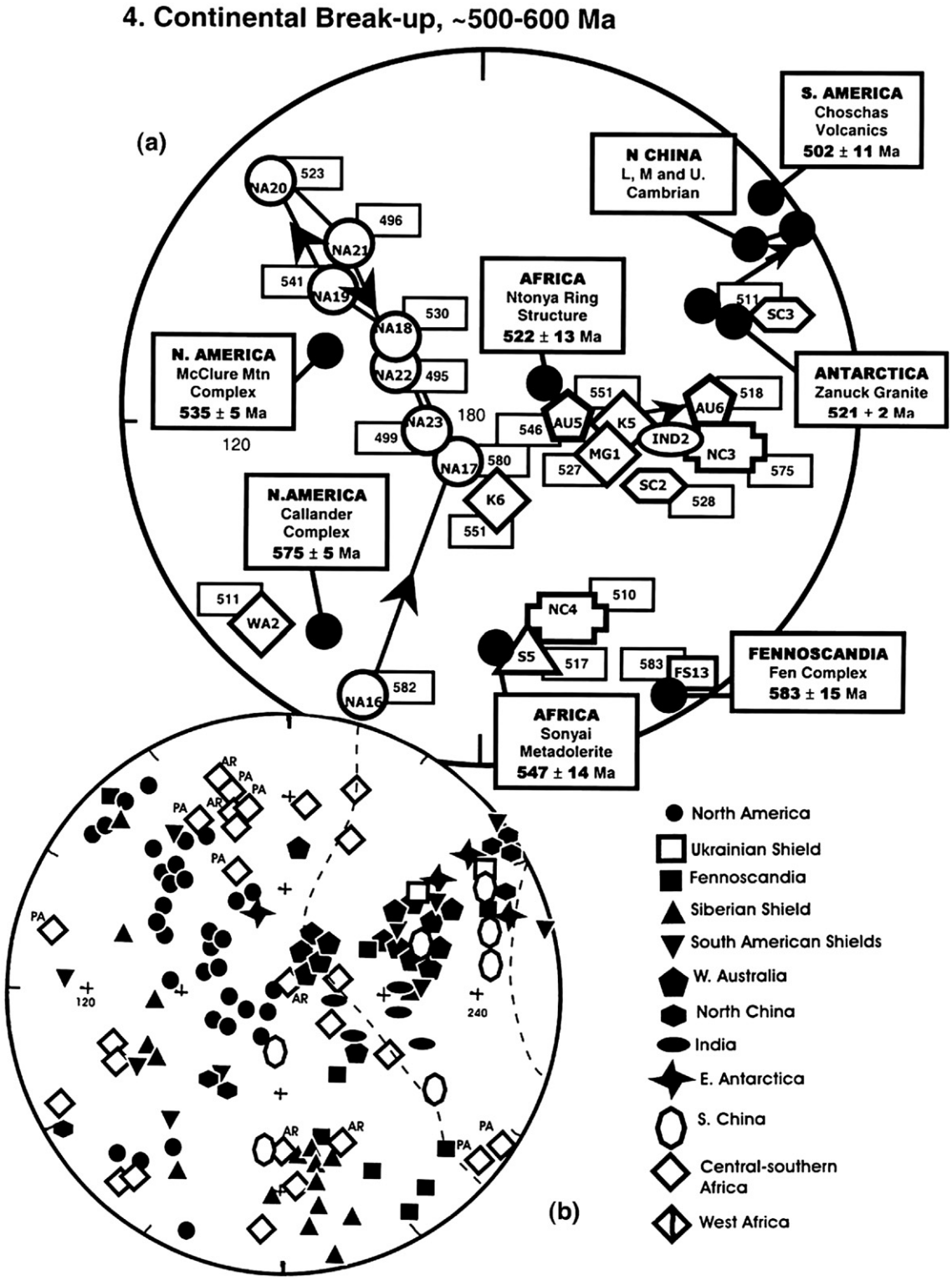


Fig. 5. (a) Summary of mean palaeomagnetic poles assigned to the interval 600–500 Ma rotated into a Laurentian reference frame according to Palaeopangaean parameters. (b) Individual poles assigned to this time window (Table 1). The dispersion of the 600–500 Ma poles using the Palaeopangaean reconstruction is the classic palaeomagnetic signature of continental break-up and emphasises that this reconstruction (continental outline shown by the dashed line) ceased to be relevant at ~600 Ma (Section 4.3).

West African and South American cratons are essentially conservative and suggest that relative movements involved in Pan African suturing were limited in scale.

South China is introduced in the secondary (<1100 Ma) reconstruction following Zhang and Piper (1997) in a configuration derived by matching younger palaeomagnetic

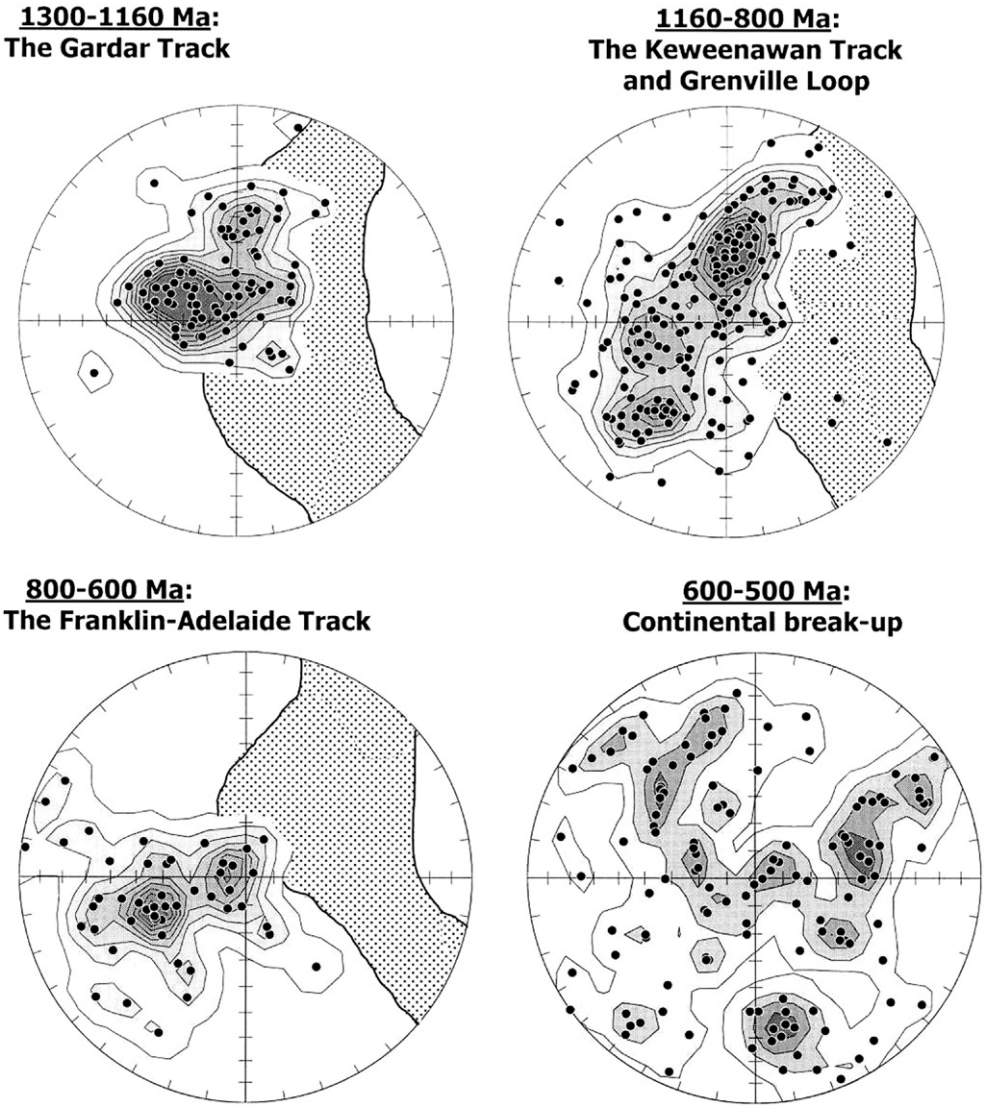


Fig. 6. Summary of the contoured distributions of poles embracing the time periods of Figs. 2–5. Note the random distribution and inferred break-up of Palaeopangaea between 600 and 500 Ma. The stippled areas are continental crust.

data from South China with the swathe of Neoproterozoic–Early Cambrian poles from the Adelaide System and Amadeus Basin in Australia (Klootwijk, 1980). North China is included in the primitive reconstruction (pole NC1 in Table 1) by matching ~1250 Ma data with the Mackenzie–Jotnian distribution whilst the secondary reconstruction of this block is again derived by matching the Neoproterozoic–Early Cambrian record with the Adelaide–Amadeus record from Australia (Klootwijk, 1980; Piper and Zhang, 1997). The secondary reconstructions of North and South China Shields imply a regional location near the northern margin of Gondwana consistent with biogeographic data (Burrett et al., 1990) whilst the suture zone between the Cathaysian and Yangzi blocks comprising South China and recognised as an Early Neoproterozoic suture zone (Zhou et al., 1993; Li et al., 1995) is then brought into continuity with the Albany–Fraser and Musgrave mobile belts of Australia.

The Siberian configuration adjacent to the western margin of North America uses the reconstruction of Sears and Price (1978, 2000). Whilst this proposition is obviously not unique, the geological case has survived the test of time and it crucially brings key 1100–1050 Ma poles from this shield into conformity with the latter part of the Keweenawan Track at ~1050 Ma; it also serves to produce crustal continuity between Laurentia–Fennoscandia and the proto-Gondwana crust (Fig. 1). The pre-1100 Ma and post-1100 Ma reconstructions of Fennoscandia follow previous studies (Patchett et al., 1978; Piper, 1980a; Stearn and Piper, 1984; Elming and Mattsson, 2001) and are currently the best palaeomagnetically-constrained facet of the reconstruction. Geological and palaeomagnetic data appear to identify differences between the Ukrainian and Fennoscandian shields at 2000–1850 Ma with probable suturing between them sometime between 1850 and 1350 Ma (Elming et al., 2001). The 1300–1000 Ma Ukrainian data (Table 1) are compatible with the APW path derived from elsewhere within their rather broad age constraints (Fig. 2) but no subsequent data from this block are acceptable until the Neoproterozoic–Cambrian boundary.

The cratonic contributions to the dataset in Table 1 are: North America 34%, Hebrides 1%, Greenland 6%, Fennoscandia–

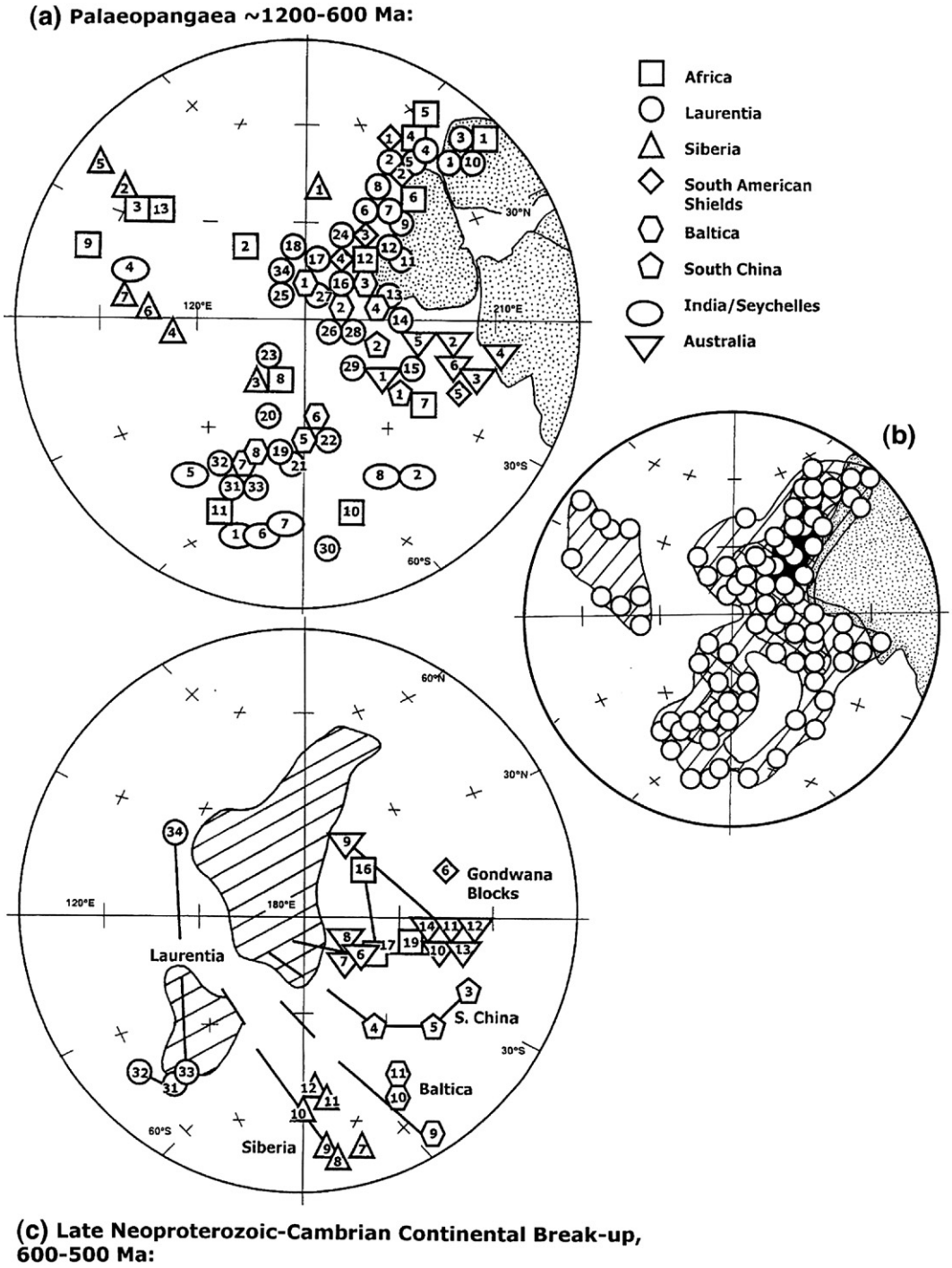


Fig. 7. The ~1250–500 Ma palaeomagnetic data selection of Meert and Torsvik (2003) rotated into the Palaeopangean reconstruction to illustrate the break-up of the supercontinent at ~600 Ma. For a key to the poles see Meert and Torsvik (2003) and Piper (2004).

Ukraine 18%, Siberia 7%, South America 3%, India/Seychelles 3%, Antarctica 1%, Africa/Arabia/Madagascar 12%, Australia 8%, South China 3% and North China 4%.

3.2. The Mackenzie–Gardar track, 1300–1140 Ma

This APW track is anchored at ~1267 Ma by palaeomagnetic results from the Mackenzie igneous province embracing shield-wide dyke emplacement in North America and the Jotnian Province of the Fennoscandian Shield collectively recording one of the most important LIP episodes in the geological record (Yale and Carpenter, 1998). The following time interval is only recorded in North America by the Abitibi dykes but is defined elsewhere by three successive pulses of igneous activity within the Gardar Province of South Greenland defining the Gardar Track (Piper, 1992). As shown in Fig. 2 it continues to the ~1140 Ma pole from the Ilímaussaq Complex, the youngest palaeomagnetically-studied event in this province (Piper et al.,

Table 2
Eulerian rotation operations used to derive Palaeopangaea

	Primitive reconstruction:			Secondary reconstruction:		
Crustal block	°E	°N	Rotation	°E	°N	Rotation
Fennoscandia (Baltica)	8.0	21.0	41.0	274.0	80.5	−66.5
Greenland	266.2	70.7	−18.1	–	–	–
Hebridean Craton	27.7	88.4	−38.1	–	–	–
Siberia	309.0	66.0	86.0	–	–	–
Guyana/Amazonia	246.5	−33.0	142.0			
Sao Francisco/ Rio de la Plata	277.0	56.0	−128.8	–	–	–
West African Craton	123.5	59.0	−131.5	–	–	–
Arabia	142.4	76.6	−148.4	–	–	–
Tanzania/Kaapvaal	138.0	73.0	−146.0	–	–	–
Pan African domains	138.0	73.0	−146.0	–	–	–
Madagascar	–	–	–	103.1	74.4	−152.0
Seychelles	–	–	–	330.2	50.5	−134.9
India	152.0	−27.5	152.0	142.0	−48.0	160.5
Australia	120.0	−84.5	−119.9	180.0	−63.5	158.3
East Antarctica	147.5	−23.0	87.8	33.7	73.1	−149.1
South China	–	–	–	279.1	58.0	−155.8
North China	26.0	−7.0	−149.0	298.0	46.5	−147.0

Footnote: Assignments 'primitive' and 'secondary' refer to configurations before and after approximately 1100 Ma. Cratonic units in the core of the reconstruction were apparently not palaeomagnetically influenced by these adjustments and have invariant operations.

1999) and the presently defined extremity of the track. Anchor poles defining the beginning of the trajectory include results from the Mackenzie LIP (1267±2 Ma), the Jotnian LIP (1245±20 Ma), and units in Greenland comprising the Grønnedal–Ika Complex (1299±17 Ma), BD0 dyke swarm (1284±3 Ma), Lamprophyre dyke swarm (1250±18 Ma) and the Kungnât Fjelt Complex (1219±16 Ma). The subsequent track is an S-shaped APW path which incorporates all the remaining acceptable global poles assigned to this interval and is specifically defined by successive anchor points comprising the Bangemall Sills of Australia (1171±8 Ma), the South Qôroq Complex of Greenland (1160±8 Ma) the Nova Floresta Formation of Amazonia (1199±5 Ma), the Abitibi Dykes (1141±2 Ma) of North America and the Ilímaussaq Complex of Greenland (1143±21 Ma). The northeasterly migration of APW in the central part of the track is recorded within the Stoer Group (1199±70 Ma) of the Hebridean Craton (Darabi and Piper, 2004).

The 'primitive' reconstruction used in Fig. 2 and defined by the parameters of Table 1 suggests a continuing proximity of the Archaean–Early Proterozoic cratons consistent with the view that no wide dispersal of Africa–Antarctica–Australia–India actually occurred prior to the break-up of (Neo)Pangaea in Mesozoic times. The recognition of ages of consolidation, uplift and supracrustal cover supports proximity between the most ancient cratonic nuclei of southern Africa, Western Australia and central-east India from 3300–300 Ma in the protocontinent of 'Ur' (Rogers and Santosh, 2004). An implausible facet of the conventional Rodinia reconstruction has thus been the wide separation of southern Africa from Western Australia–India in Neoproterozoic times to be followed by their rapid reunification into Gondwana by Early Palaeozoic times. The present analysis suggests that no such history actually occurred. The other two Archaean–Early Proterozoic nuclei identified by Rogers (1996) comprise 'Arctica' (Fennoscandia–Laurentia–Siberia) with apparent integrity originating at ~2500 Ma and 'Atlantica' (Guyana–Sao Francisco–West Africa) with a common history dating from 2200–2000 Ma and supporting the early proximity of South American and West African cratons in Palaeopangaea. The continuing proximities of these nuclei in Late Mesoproterozoic times within the reconstruction used here favours a quasi-integral interpretation of Proterozoic crustal geometries; it specifically overcomes the acute geometrical problem posed by the Rodinian requirement for the South American shields to be rapidly transferred to the opposite side of the reconstruction by early Phanerozoic times.

3.3. The Keweenawan track and Grenville–Sveconorwegian loop, 1140–800 Ma

The return track of an APW loop recorded in the Keweenawan Province has been known in outline for many years and connects, probably by an east–west track, to an APW loop recorded by Grenville and Sveconorwegian magnetisations. In general terms the Keweenawan Track appears to follow a path close to the outward Gardar Track although in detail the contributions of APW and reversal asymmetry over the central part of this trajectory are unresolved (Schmidt and Williams, 2003). In the combined version of the track shown in Fig. 3 the south westerly migration of APWP is well defined in Laurentia by the successive sequence of key anchor poles including the Coldwell Complex (1108±1 Ma), the Logan Sills (1108±4 Ma), the Duluth Gabbro (1091±14 Ma), the Cardena Volcanics (1091±5 Ma), the Portage Lake Volcanics (1096±2 Ma) and the Lake Shore Volcanics (1087±2 Ma) with these latter studies identifying asymmetry of reversal in dual polarities and suggesting possible non-dipolar contributions to the geomagnetic field source (Nevanlinna and Pesonen, 1983). Within Africa the same polar migration is defined by anchor poles comprising the Umkondo lavas and dolerites (1105±2 Ma) and the post-Waterburg Dolerites (1091±15 Ma) moving to the O'okiep intrusions (1020±30 Ma) along a trend that also includes the Group de Char (1019±32 Ma) from West Africa. In the Sao Francisco craton identical APW is defined between poles from the Olivenca Dykes (1078±18 Ma) and the Ilheus Dykes (1012±24 Ma). Anchor poles from the southern wing of the reconstruction comprise the Coats Land Nunataks pole from Antarctica (1112±4 Ma) plotting at the predicted position near the apex of the loop joining the Gardar and Keweenawan tracks and the Kulgera Dyke pole from Australia (1054±14 Ma) lying near the middle of the track close to poles of comparable age from elsewhere; poles summarised as AU2 in Table 1 from the Mt Isa Belt at the margin of cratonic Australia show no correspondence with the data from elsewhere and are possibly allochthonous.

The clockwise or anticlockwise character of the succeeding Grenville–Sveconorwegian Loop has been much debated (see Weil et al., 1998 for discussion). A tight anticlockwise loop based on "chrontour" uplift and cooling ages from the Grenville Province (McWilliams and Dunlop, 1978) is likely to be

unreliable in detail because hydrothermal alteration has caused chemical remagnetisation and anomalously old K/Ar ages near the Grenville Front (Constanzo Alvarez and Dunlop, 1998). Recent revision of the contemporaneous record from the Fennoscandian Shield (Pisarevsky and Bylund, 1998; Piper, in press) suggests that the APW motion was southeasterly from the ~1020 Ma pole FS5 to the earliest (~975 Ma) record within the Sveconorwegian Belt (FS6) and was succeeded by a clockwise return path as shown in Fig. 3a. Loops from the two shields conform when Fennoscandia is restored to a position adjacent to the Grenville margin of Laurentia (Patchett et al., 1978; Piper, 1980a and Fig. 1).

Part of this loop is also recorded within the Bukoban Supergroup of central Africa (Piper, 1980a) although pole T1 from this succession and mean pole NC2 from supracrustal rocks of North China plotting at the southerly extremity of the loop are dated approximately 100 Ma younger than coincident poles from the Grenville and Sveconorwegian belts. This is possibly due to the difficulty of assigning precise ages to magnetisations acquired during slow crustal exhumation and cooling of the orogenic belts; it may explain why the magnetisation in the Tudor Gabbro within the Grenville Province (included in mean pole NA9 in Table 1) has a position indicating an age some 100 Ma younger than the assigned age of 1110±20 Ma (unless this body is allochthonous, see Warnock et al., 2000). Age estimates from the supracrustal rocks are thus probably closer to the true age of the extremity of this loop. This age discrepancy cannot reflect a failure of the quasi-rigid model at this point because the subsequent key anchor poles assigned to the interval 800–600 Ma continue to conform tightly to a single track using the same rotational parameters as the pre-1000 Ma data (c.f. Figs. 3 and 4). Results from the Siberian Shield incorporated in this time interval comprise seminal studies of the Linok and Malgina successions dated ~1050 Ma which correlate with the contemporaneous (younger) part of the Keweenawan Track using the Sears and Price (2000) reconstruction; four poles from the Turukhansk, Slyudyankinskaya, Kandykshaya and Ust–Kirbinskaya Suites plot to the east of the Grenville–Sveconorwegian Loop (Fig. 3b) and removed from other poles assigned to their rather broad age range (~1100–820 Ma); however their antipoles correlate with the path at ~800 Ma (Fig. 4) suggesting that the magnetisations are somewhat younger than the assigned formation ages.

3.4. The Franklin–Adelaide track, 800–600 Ma

The data from diverse continental blocks assigned to this interval conform remarkably closely to a unified southeast trending APW path (Fig. 5) using the same reconstruction as Fig. 3 and the core continental configurations in Fig. 2. Since this path includes the Franklin LIP in North America and Greenland, and the latter part incorporates the stratigraphic succession of poles from the Adelaide Geosyncline of Australia, it is referred to here as the 'Franklin–Adelaide Track'. In the South China block the southeast APW trend is identified between poles from the Xioafeng dykes (802±10 Ma) and the Nantuo Glacial rocks, with the latter now dated between 663 and 559 Ma in age (Zhou et al., 2004). In the Fennoscandian Shield on the opposite wing of the reconstruction the identical APW trend is present between poles from the Vadsö/Barents Sea/Kola successions (~770 Ma, mean pole FS13 in Table 1) and the Varangian interglacial (Nyborg Formation, 653±7 Ma). In the Indian Shield the same trend is identified between poles from the Harohalli dykes (832±14 and 823±15 Ma) and the Malani Igneous suite (771±2 Ma and 751±3, c.f. Torsvik et al., 2001a), a trajectory that also incorporates anchor poles from the Mahe Granite (755±1 Ma) and dykes (750±3 Ma) from the Seychelles Microcontinent when rotated into a position adjacent to eastern India (Torsvik et al., 2001b). In Australia the same APW trend continues between poles from the Mundine Dykes (755±3 Ma) and the Elatina periglacial rocks (~620–600 Ma). Anchor poles from other continental blocks plotting close to predicted positions on this APW path include the Mbozi Complex of Central Africa (743±10 Ma), the Franklin LIP (723±3) of North America and the La Tinta Formation of South America (709±24 Ma), although the latter is shifted somewhat to the south west (Fig. 4a). The unified APW track terminates in poles from glaciogenic facies assigned to the Marinoan including the Nantuo of South China, the Elatina of Australia (610±10 Ma) and the Varangian of Norway (653±7 Ma) with the approximate age of this latter part of the track independently confirmed by coincidence with the pole from the Adma Diorite of West Africa (613±3 Ma).

The tight conformity of poles from diverse continental shields to a single APW path during the 800–600 Ma interval is crucial to testing between the Palaeopangaean and Rodinian hypotheses. All Rodinian models invoke relative movements between the continental blocks during these times and require that APW paths of the different cratons are of variable lengths and shapes. In the event the poles from this interval are found to conform to a unified APW path with the key anchor poles plotting at locations according with their assigned ages (Fig. 4). It is thus unnecessary to invoke continental break-up prior to 600 Ma and, as discussed in Section 4, this key observation produces convergence of important geological and geophysical observations.

3.5. The Eocambrian continental break-up

The grouping of poles from Marinoan-age glacial units in Fig. 4 is the last point at which the unified APW path identifies quasi-rigid integrity of the continental crust. After ~600 Ma the poles explicitly scatter and show the classic palaeomagnetic signature of continental break-up (Fig. 5). The nature of APW in the latest Neoproterozoic and Cambrian has been evaluated by a number of authors (e.g. Kirschvink et al., 1997; Smethurst et al., 1998; Meert, 1999) and is only outlined here in the context of rotation following Palaeopangaean parameters. The key observation to emerge from comparison of Figs. 2–4 with Fig. 5 and the contoured distributions in Fig. 6 is that the reconstruction embraced by the Neoproterozoic palaeomagnetic analysis ceases to be valid after 600 Ma. The dispersal of poles from diverse shields thus reconciles palaeomagnetic interpretation with the time of continental break-up predicted from the geological evidence (Bond et al., 1984) and surmounts the most important difficulty posed by the Rodinia hypothesis. Anchor

poles from the Callander Complex of North America (575 ± 5 Ma) and the Fen Complex of Fennoscandia (583 ± 15 Ma) for example, become widely divergent (Fig. 5) as they record the opening of the Iapetus ocean initiated at ~595 Ma (e.g. Halliday et al., 1989). In general terms the North American poles then move to the north and west, poles from Siberia plot close to those from North America suggesting that the two blocks may not have drifted far apart during the Cambrian, and Gondwana poles move to the east and northeast. In detail some of the Gondwana poles are highly divergent (Fig. 5b) although data failing to conform with the general easterly trend are mostly from Arabian and Pan African terranes (denoted AR and PA in Fig. 5b) and are possibly allochthonous.

Following the movement to the southwest, subsequent North American poles assigned to the interval 570–495 Ma are consistent with the outward and return limbs of a tight loop and have been organised to demonstrate this in terms of the mean poles listed in Table 1 and plotted in Fig. 5. Within the age uncertainties this is of course, not a unique solution and an alternative explanation is described by Meert (1999). Whilst this APW was occurring relative to Laurentia, other shields were following independent paths: on the projection of Fig. 5a the Fennoscandian path moves to the southeast (FS13) and then northeast. African poles probably describe a large loop which takes the path to the top of this projection to incorporate poles such as the Nama Group (~570 Ma) and then returns near to the ~600 Ma position by 522 ± 13 Ma to the anchor pole from the Ntonya Ring Structure of Malawi. During this time interval South America poles are expected to follow those from Africa closely although subject to relative motions on the Pan African belts and compatible with the limited dataset (Table 1). Poles from the other Gondwana blocks indicate smaller motions to the east (Fig. 5a) where a position near the north east primitive incorporates Lower to Upper Cambrian poles from China.

Numerous workers have recognised large APW movements in the Cambrian data and Kirschvink et al. (1997) suggest that an episode of inertial interchange true polar wander (IITPW) at ~525–505 Ma is responsible. Meert (1999) argues against this possibility because APW motions are less than 90° and apparently differ from block to block. The analysis of Fig. 5 does not discount a contribution of TPW to observed APW but identifies continental break-up as the cause of the diverse APW paths leading to the random distribution of poles by 600–500 Ma as shown in Fig. 6. Furthermore there are reasons to suspect that movements would have been rapid during these times since the break-up event was associated with igneous provinces, which in the case of North America involved the rise of one or two plumes (Doig, 1970; Higgins and van Breemen, 1998). Gurnis and Torsvik (1994) propose that motions are enhanced when continents with significant lithosphere roots move away from long-wavelength geoid highs generated by such hot lower-mantle sources.

The validity of the Palaeopangaean reconstruction and its fragmentation after 600 Ma are demonstrated in two additional ways in Figs. 6 and 7. The contoured distributions of the palaeomagnetic poles plotted in Figs. 2–5 illustrate tight groupings between 1300 and 600 Ma succeeded by a distribution which is essentially random between 600 and 500 Ma as the supercontinent was being dismembered (Fig. 6). Fig. 7 shows that the most important conclusion of this analysis, namely that the supercontinent was quasi-rigid prior to 600 Ma and dismembered after 600 Ma, does not depend on the data selection used here. The polar compilation used by Meert and Torsvik (2003) to develop a Rodinia case is separated into groupings of ~1250–600 Ma and 600–500 Ma data. Most of these poles are included in the unified path described in Figs. 2–4. The dispersal of poles after 600 Ma is evident and comparable to that recognised in Figs. 5 and 6.

4. Geological and geophysical implications

Many of the geological and geophysical implications of the Palaeopangaean reconstruction have been developed elsewhere (Piper, 1980a, 1982, 1987, 2000). Other ramifications not yet addressed but beyond the scope of this paper include the nature of the geomagnetic field source and the distributions of Neoproterozoic glaciation and Ediacaran faunas. The focus of this contribution is the pressing need to clarify Neoproterozoic palaeogeography and analysis is limited to comments in four areas, namely the link to the geoid form, the distribution of Neoproterozoic orogenesis, the explanation of the threefold cyclic deposition of megasequences that has played such an influential part in formulating the Rodinia hypothesis, and the link between break-up of Palaeopangaea and isotopic signatures.

4.1. Continental shape and relationship to the Geoid

The Phanerozoic supercontinent Pangaea (Wegener, 1923) possessed a number of geometrical properties. The overall crescent form comprised two wings of approximately equal continental area constrained within a great circle perimeter, which at least during the latter part of its history (~300–125 Ma), passed through the palaeopoles of rotation (Gough, 1977; Le Pichon and Huchon, 1984 and Fig. 8). An eastward-expanding ocean, the Tethys, separated the two wings and possessed a circulation that was controlled by the latitudinal orientation and a continental bridge between the Eurasia and Gondwana arcs of the crescent. The great circle periphery comprised the western Palaeopacific subduction zone and extended from the palaeoequator towards the geographic poles (Le Pichon and Huchon, 1984). Obvious conformity of the Pangaean shape to the present geoid, which is dominated by low-order symmetry of "tennis-ball" shape, links the formation of this supercontinent to density variations within the deep mantle and is presumably caused by convective heat release from the Earth's interior. Parallels between the geoid form and Pangaean shape support the view that large-scale mantle convection operates, at least episodically, to aggregate continental crust into a body with specific geometrical properties reflecting the geoid topography (Gough, 1977). It has been speculated that the supercontinent subsequently acts as a lid over the underlying mantle to steepen temperature gradients and lead to catastrophic thermal changes in which lie the seeds of its own break-up and dispersal (Anderson, 1982).

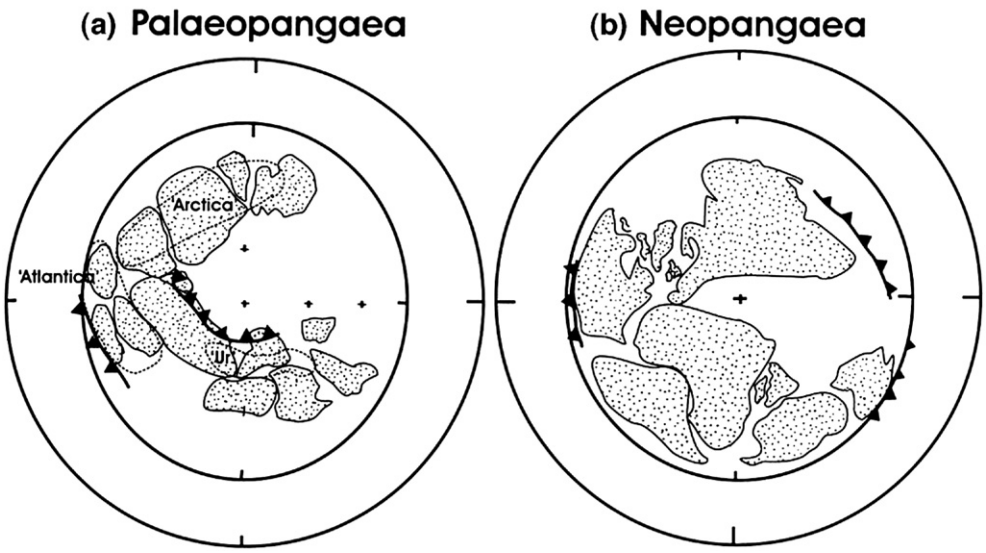


Fig. 8. Comparative reconstructions of Palaeopangaea and Neopangaea oriented into single hemispheres of a Lambert equal area projection of the whole globe to illustrate their comparable symmetrical and crescent shaped forms. 'Ur', 'Arctica' and 'Atlantica' are assemblages of cratons with similar Archaean–Palaeoproterozoic histories (Rogers, 1996; Rogers and Santosh, 2004).

Due to the paucity of palaeomagnetic poles and/or their temporal coverage, the configurations of smaller blocks within the Palaeopangaean reconstruction are unknown. Nevertheless, the reconstruction to emerge from present data defines a crustal configuration that is remarkably similar in form to Wegener's Pangaea (referred to hereafter as 'NeoPangaea'). In each case there are two wings of approximately equal area separated by an ocean, and an outer rim with a perimeter conforming broadly to a great circle (Fig. 8). It is therefore inferred that Neoproterozoic crust was constrained onto the Earth's surface by large-scale forces comparable to those reflected in the contemporary geoid and in Neopangaea. In the present Earth the geoid positive is oriented on average into the equatorial plane to minimise the kinetic energy of rotation and the continental crust, with the exception of a near-stationary Africa, is moving towards the geoid negative region (Le Pichon and Huchon, 1984). Thus continental crust, probably due to a thick lithosphere root, is influenced by deep geoid-related convection (Gurnis and Torsvik, 1994) whereas plates covered mostly, or entirely, by oceanic crust show no such relationship because they are driven by shallow convection powered by ridge-push and slab-pull forces (Davies, 1999).

There are contrasting views about the geometry of mantle convection reflected in the geoid form (Gough, 1977; Besse, 1983; Le Pichon and Huchon, 1984). It was expressed around the outer margin of Neopangaea as the Palaeopacific subduction zone but appears to have been concentrated at the opposite margin of Palaeopangaea within the instep of the reconstruction (Fig. 8). The Afro–Arabian sector extending southwards to Mozambique was the focus of subduction and orogeny in the Neoproterozoic (Stern, 1994; Meert, 2003) and was characterised by calc-alkaline magmatism until the late Neoproteozoic continental break-up when a magmatic transition reflected the transformation in tectonic regimes by converting from calc-alkaline to alkaline (Harris and Gass, 1981). In Fig. 8 the generalised form of this arc is extended southeast to include the Neoproterozoic calc-alkaline Malani Province of NW India. This Neoproterozoic magmatism and orogenesis was evidently marginal and linked to subduction of ocean crust; marginal orogenesis also appears to have been taking place at the opposite margin of the supercontinent in the Late Vendian to Early Palaeozoic Pampean Orogeny (Acenolaza et al., 2000) where it followed the Susnas Orogeny of Grenville age deformation along the margin of Amazonia.

4.2. Meso–Neoproterozoic orogeny and sedimentation

The proposed linkage of ~1100 Ma 'Grenville' orogenic belts of Hoffman (1991) was most importantly constrained by the stratigraphic link between Australia, South China and western North America and was clearly non-unique. The Palaeopangaean reconstruction implies that these belts instead formed an en echelon system following the symmetrical arcuate shape of the supercontinent (Fig. 9). Continuity was present between the Sveconorwegian and Grenville belts prior to late Mesoproterozoic break-up of the Laurentian and Fennoscandian Shields (Patchett et al., 1978; Piper, 1980a; Elming and Mattsson, 2001). Whilst the possible southwest continuation of the Grenville Belt into Mexico is unclear (Rogers and Santosh, 2004), the trend continues into central Africa (Piper, 1980a). A direct link is unlikely specifically because the western (Kibaran) belt has a sharp westward deflection at its northern extension although the Kibaran and Irumide belts are predicted to continue southwards on the opposite side of the Damaran–Lufillian (Pan African) orogeny into the Natal Belt and thence into the Rayner Belt of Antarctica, the Eastern Ghats of India and the Albany, Fraser and Musgrave belts of Australia. Whilst there is collective continuity, these belts individually have a complex history (e.g. Fitzsimons, 2000) involving collision and transpression and their initial geometry will only be clarified when the late Mesoproterozoic motions translating

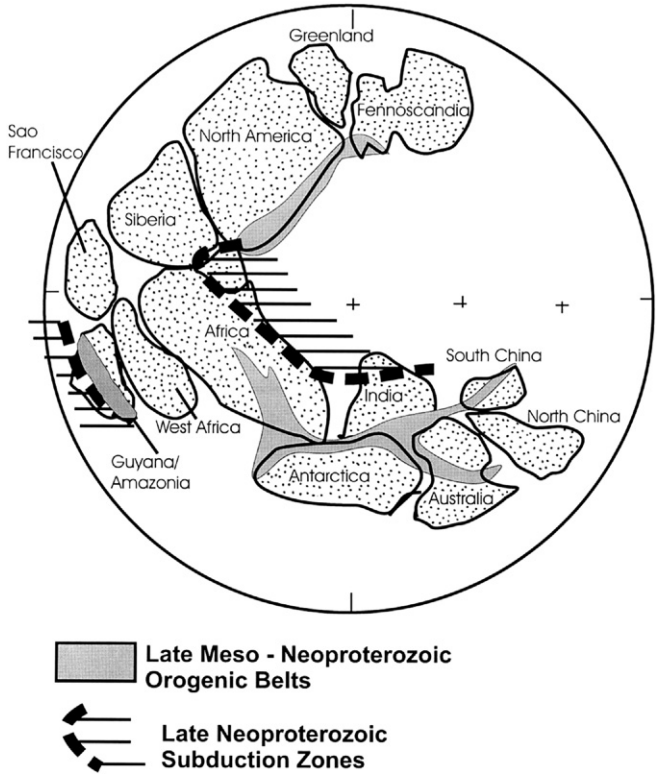


Fig. 9. The distribution of Late Mesoproterozoic–Early Neoproterozoic orogenic belts linked to the Grenville episode and the approximate region influenced by calc-alkaline arc-related magmatism and subduction between ~750 Ma and the break-up of the supercontinent shortly before the beginning of Cambrian times.

the crust from the primitive to the Neoproterozoic reconstructions are defined (i.e. the transition between the configurations of Figs. 2 and 3, and see also Fig. 1). The Palaeopangaen solution predicts that most of these belts were peripheral to the supercontinent although the examples in central Africa seem to have been essentially intracratonic. An implication of the analysis is that the ~1100–1000 Ma Sunsas Belt, which extends along the western margin of the Amazonian Shield southwards into Bolivia and thence beneath the Andean Orogen, developed at the opposite margin of the supercontinent from the Grenville and Sveconorwegian belts and appears to have had no direct linkage to them (Fig. 9).

The relative continental movements forming Gondwana by early Phanerozoic times and embracing the interval of Pan African orogenesis (for recent review see Meert, 2003) are identified as mainly transpressive in character (Figs. 8 and 9) in conformity with the views of Dewey and Burke (1973), Coward and Daly (1984) and Stern (1994). Commenting that no direct exposure of a continental suture had yet been resolved in southeastern Africa, Li and Powell (1993) noted the importance of left-lateral oblique collisions along the Mozambique Belt. The broadly ensialic character of this zone is emphasised by the strong Archaean affinities between Australia, India and southern Africa (Wingate, 1998; Zegers et al., 1998; Rogers and Santosh, 2004).

A corollary of this analysis is that the large scale threefold lithological repetition in Neoproterozoic successions that formed the original basis of the Rodinia reconstruction (Eisbacher, 1985; Bell and Jefferson, 1987; Dalziel, 1991; Moores, 1991) is not relevant to their spatial proximities. An alternative explanation is that these transgressive–regressive cycles are eustatic in origin and a consequence of TPW: when a continent is moved into lower latitudes it is subject to rise in sea level because the ocean adjusts to the lower gravitational potential immediately whereas the mantle and lithosphere response lags behind (Mound and Mitrovica, 1998). As the load on the mantle and lithosphere relaxes the sea level adjusts to its initial position over a time period dependent on the interval of TPW and the viscosity profile in the upper mantle.

The three sedimentary divisions in Eastern Australia, North America and South China were deposited during an interval of time embraced by an APW loop presumably executed shortly before 800 Ma and comprising the link between the end of the Grenville–Sveconorwegian Loop and the beginning of the Franklin–Adelaide Track (Figs. 3 and 4). The motion recorded by this loop carried North America into lower latitudes (transgression) prior to Franklin times at which stage poles NA15 → NA16 imply motion of western North America back into higher latitudes (regression) and then back to lower latitudes (pole NA17, transgression) by the beginning of the Cambrian. As recorded in South China this latter motion could include migration between the Xiaofeng and Nantuo poles that carried this block from higher to lower latitudes (transgression), with the Nantuo formation defining the end of the second sedimentary cycle. Thus after deposition of the first (Rapitan) cycle, which is mainly diamictite, continental motions embraced by the Franklin–Adelaide Track are probably able to explain sedimentary cycles 2 and 3 before the Neoproterozoic–Early Cambrian boundary, with the latter boundary occurring within the higher part of the third cycle (Eisbacher, 1985).

4.3. Late Neoproterozoic continental break-up and isotopic signatures

Tectonic subsidence curves derived from the Early Palaeozoic passive marginal successions extrapolate backwards to predict a global continental break-up event between ~600 and 560 Ma (Bond et al., 1984). This correlates with transition from the integral supercontinent at 600 Ma to dispersed continents between 600 and 550 Ma as shown in Figs. 5 and 6 and was accompanied by widespread intracontinental alkaline magmatism (Doig, 1970; Piper, 1987); the geological evidence and predictions of the Palaeopangaean analysis converge on this key point. The formation of hot and buoyant spreading ridges during break-up and the stretching and attenuation of new continental margins would have combined to cause of the flooding of Cambrian shelves. Initial deposits were poorly fossiliferous arenitic sands, but as the shelf areas expanded there was increasing scope for biological diversity, which is evidently, linked to the increase in metazoan families; subsequent dispersion of the continents promoted provinciality (Conway Morris, 1987).

Isotopic signatures of this break-up event are summarised in Fig. 10 to show their striking correlation with the break-up of

Palaeopangaea. Their collective implication is clear although the individual isotope systems are complex and may have a variety of interrelated causes. A large negative shift in $\delta^{13}C$ (i.e. an increased proportion of lighter ^{12}C) occurred before break-up (Fig. 10) and has been interpreted as a reduction in ocean productivity (Knoll et al., 1986; Magaritz et al., 1986) because organic matter preferentially incorporates ^{12}C. This is a global event and has been attributed to stagnant ocean conditions during warm climates following the last Neoproterozoic glaciation

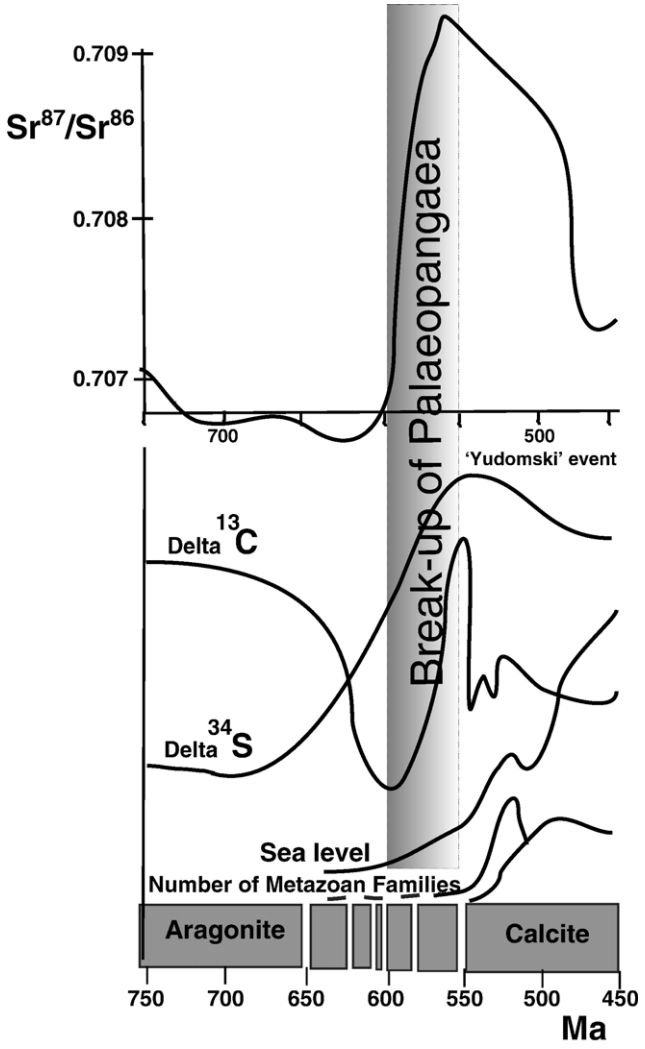


Fig. 10. Geological, biological and chemical trends spanning the Late Neoproterozoic–Phanerozoic boundary adapted, with additions, from Conway Morris (1987). There is marked increase in the number of Metazoan families across the boundary from a Precambrian distribution that is low but uncertain; the peak in numbers in the Lower Cambrian is primary attributed to the archaeocyathids and the lower line applies to metazoans with these excluded. The sea level curve records the Cambrian transgressions punctuated by the Hawke Bay regression near the Lower–Middle Cambrian boundary. Changes in geochemistry (Holser, 1977; Knoll et al., 1986; Veizer, 1989; Condie, 1997) include the variation in minimum $^{87}Sr/^{86}Sr$ ratios derived from marine carbonates are of enigmatic and probable complex origin (see text). The ^{32}S to ^{34}S ratio near the boundary includes the Yudomski Event inferred to be due to input of large volumes of evaporates into the oceans and upwelling of deep waters as enclosed basins were destroyed by break-up; this in turn fed large amounts of phosphorus to shallow waters. Complex shifts in the ratio of ^{12}C to ^{13}C ($\delta^{13}C$) may reflect increases in oceanic productivity.

leading to dyoxic deepwater enriched in nutrients (Kimura et al., 1997). Subsequently massive up welling of deepwater caused enhanced phytoplankton productivity accompanying the break-up of Palaeopangaea and development of new oceans. The increase in $\delta^{13}C$ during the break-up is attributed to the combined effect of increased organic activity and enhanced sedimentation in shallow seas (Kimura et al., 1997); increased erosion could also have contributed (Condie, 1997) although this is more likely to have been a consequence of Pan African orogenesis. The $\delta^{13}C$ peak in Fig. 10 has been related to the Yudomski Event (Conway Morris, 1987) with the latter opening up an ecological niche.

The partial pressure of carbon dioxide (pCO_2) controls carbonate precipitation with calcite favoured by increased pCO_2 flux and aragonite by lower fluxes. The transition from aragonite to calcite at the Neoproterozoic–Cambrian boundary must ultimately reflect growth of new ocean basins because the flux of CO_2 into the oceans increases during periods of rapid spreading. Metamorphic reactions in subduction zones release CO_2, which is then channelled to the surface through volcanic activity. Two accompanying effects also work to increase pCO_2: marine transgression inhibits continental weathering that would otherwise consume CO_2 and hydrothermal weathering at ocean ridges removes Mg and adds Ca to increase the Ca/Mg ratio of seawater (Conway Morris, 1987; Condie, 1997).

The largest fluctuation in the ratio of sulphur isotopes ^{32}S and ^{34}S (expressed as $\delta^{34}S$) in the geological record is the Yudomski Event (Holser, 1977) which correlates with the break-up of Palaeopangaea (Fig. 10). This ratio depends on the balance between bacterially controlled precipitation of pyrite in anoxic sediments and the oxidation of sulphides elsewhere. The signature at the Neoproterozoic–Cambrian boundary is attributed to the catastrophic release of brines, which had accumulated in anoxic conditions within enclosed basins immediately prior to break-up, into the oceans as the continents broke apart (Holser, 1977; Piper, 1987; Conway Morris, 1987). This release of brines into the oceans would also have added large amounts of nutrients and phosphorous to enhance the productivity of the new marine shelves and account for the widespread phosphorite deposits of this age (Cook and Shergold, 1984).

The break-up of Palaeopangaea correlates with the largest single increase of the $^{87}Sr/^{86}Sr$ ratio in the geological record (Fig. 10) and merits comparison with a comparable but smaller increase observed after 150 Ma correlating with break-up of Neopangaea (Veizer, 1989). In each case continental break-up and new ocean formation was broadly synchronous with orogeny and continental uplift, in the former case this is the Pan African Orogeny and in the latter case the Alpine–Himalayan Orogeny. However, the relationship of $^{87}Sr/^{86}Sr$ ratios derived from marine carbonates to supercontinent formation is not fully understood (Condie, 1997). It has been tacitly assumed that increase in the number of ocean ridges between dispersing continents injects more mantle Sr into the ocean system and causes the ratio to decrease (Yale and Carpenter, 1998). Peaks in the $^{87}Sr/^{86}Sr$ curve have been attributed to an enhanced continental contribution by rivers with the suspicion that this should be greater during supercontinent episodes. However, river waters flowing from young orogenic terranes have been found to be strongly

radiogenic (Quade et al., 1997) indicating that the strontium ratio cannot be used as a straightforward proxy for continental silicate weathering. Thus inverse correlation with continental break-up shown in Fig. 10 remains enigmatic but would appear to be the net effect of a composite system involving new ocean basins, changing riverine patterns and destruction of marginal enclosed basins; it clearly correlates temporally with the other multiple indicators for continental break-up at 600–550 Ma.

The key observation from Fig. 10 is that all of these isotopic/environmental signatures are concentrated within the narrow time frame embraced by the break-up of Palaeopangaea and cannot be reconciled with the Rodianian models requiring break-up over a long time interval of ~800–550 Ma.

5. Conclusions

The validity of the Palaeopangaean reconstruction is palaeomagnetically testable at two levels. The most important test comes from the anchor poles linked to precise age determinations. Although there are still many temporal gaps in the records from continental shields, it is already apparent that these show a tight conformity to the single APW path (Figs. 2a–4a) with specific sequences of poles conforming to the APW trend. This is powerful evidence in the case of the quasi-rigid model because the hypothesis makes special demands on the data and requires conformity to a single path and it reinforces the case made more than 20 years ago (Piper, 1982, 1987) when the database was much less well constrained than it is today. Whilst the age assignments of some poles remain inconsistent and these have been duly noted in the above analysis, the poles older than 600 Ma continue to group to the APW path and do not disperse all over the projection as they should do if the shields were moving relative to one another. At a lower level the reconstruction is testable from the conformity of the majority of secondary poles to a simple APWP with the groupings of these poles being obviously non-random. Figs. 2b–4b and 6 demonstrate this to be the case for Palaeopangaea. The strength of the Palaeopangaean reconstruction is the long interval of time during which it does not require significant adjustment, the geodynamic significance of its shape, and its ability to accommodate a wide range of geological observations. It also surmounts the acute temporal and geometrical problems posed by the Rodinian reconstruction.

Acknowledgements

I am very grateful to Professor J.J.W. Rogers, Dr T. Radhakrishna and Dr D.N. Thomas for their constructive criticisms of the manuscript and their valued suggestions for improvements.

References

Acenolaza, F.G., Miller, H., Toselli, A.J., 2000. The Pampean and Famatinian Cycles — superposed orogenic events in West Gondwana. Sonderheft ZAG 1, 337–343.

Alkmin, F.F., Marshak, S., Fonseca, M.A., 2001. Assembling West Gondwana in the Neoproterozoic: clues from the Sao Francisco craton region, Brazil. Geology 29, 319–322.

Anderson, D.L., 1982. Hot spots, polar wander, Mesozoic convection and the geoid. Nature 297, 391–393.

Bell, R.T., Jefferson, C.W., 1987. An hypothesis for an Australia–Canadian connection in the late Proterozoic and the birth of the Pacific Ocean, Australian. Institute Mining and Metallurgy 87, 29–50.

Besse, F.H., 1983. Quadrupole convection in the lower mantle? Geophysical Research Letters 10, 285–288.

Bond, G.C., Christie-Blick, N., Kominz, M.A., 1984. Break-up of a supercontinent between 635 Ma and 555 Ma: new evidence and implications for continental histories. Earth and Planetary Science Letters 70, 325–345.

Buchan, K.L., Mertanen, S., Park, R.G., Pesonen, L.J., Elming, S.-A., Abrahamsen, N., Bylund, G., 2000. Comparing the drift of Laurentia and Baltica in the Proterozoic: the importance of key palaeomagnetic poles. Tectonophysics 319, 167–198.

Burrett, C., Berry, R., 2000. Proterozoic Australia–Western United States (AUSWUS) fit between Laurentia and Australia. Geology 28, 103–106.

Burrett, C.F., Long, J., Stait, B., 1990. Early–Middle Palaeozoic biogeogrtaphy of Asian terranes derived from Gondwana. In: McKerrow, W.S., Scotese, C.R. (Eds.), Memoir. Palaeozoic Palaeogeography and Biogeography, vol. 12. Geological Society, London, pp. 97–104.

Condie, K.C., 1997. Plate Tectonics and Crustal Evolution. Butterworth Heinemann, Oxford. 282 pp.

Constanzo Alvarez, V., Dunlop, D.J., 1998. A regional palaeomagnetic study of lithotectonic domains in the Central Gneiss Belt, Grenville, Province, Ontario. Earth and Planetary Science Letters 157, 89–103.

Conway Morris, S., 1987. The search for the Precambrian–Cambrian boundary. American Scientist 75, 157–168.

Cook, P.J., Shergold, J.H., 1984. Phosphorus, phosphorites and skeletal evolution at the Precambrian–Cambrian boundary. Nature 308, 231–236.

Coward, M.P., Daly, M.C., 1984. Crustal lineaments and shear zones in Africa: their relationship to plate movements. Precambrian Research 24, 27–45.

Dalziel, I.W.D., 1991. Pacific margins of Laurentia and east Antarctica–Australia as a conjugate pair: evidence and implications for an Eocambrian supercontinent. Geology 19, 598–601.

Dalziel, I.W.D., 1992. On the organisation of American Plates in the Neoproterozoic and the breakout of Laurentia. GSA Today 2 (11), 237–241.

Dalziel, I.W.D., 1997. Neoproterozoic–Palaeozoic geography and tectonics: review, hypothesis, environmental speculation. Geological Society of America Bulletin 109, 16–42.

Darabi, M.H., Piper, J.D.A., 2004. Palaeomagnetism of the (Late Mesoproterozoic) Stoer Group, northwest Scotland: implications for diagenesis, age and relationship to the Grenville orogeny. Geological Magazine 141, 15–39.

Davies, G.F., 1999. Dynamic Earth: Plates, Plumes and Mantle Convection. Cambridge University Press, Cambridge. 458 pp.

Dewey, J.F., Burke, K.C.A., 1973. Tibetan, Variscan and Precambrian basement reactivation: products of continental collision. Journal of Geology 81, 683–692.

De Wit, M.J., Thiart, C., Doucoure, M., Wilsher, W., 1999. Scent of a supercontinent: Condwana's ores as chemical tracers — tin, tungsten and the Neoproterozoic Laurentia–Gondwana connection. Journal of African Earth Sciences 28, 35–51.

Doig, R., 1970. An alkaline rock province linking Europe and North America. Canadian Journal of Earth Sciences 7, 22–28.

Eisbacher, G.H., 1985. Late Proterozoic rifting, glacial sedimentation and sedimentary cycles in the light of Windermere deposition, Western Canada. Palaeogeography, Palaeoclimatology and Palaeoecology 51, 231–254.

Elming, S.-A., Mattsson, H., 2001. Post-Jotnian basic intrusions in the Fennoscandian Shield, and the break up of Baltica from Laurentia: a palaeomagnetic and AMS study. Precambrian Research 108, 215–236.

Elming, S.-A., Mikhailova, N.P., Kravchenko, S., 2001. Palaeomagnetism of Proterozoic rocks from the Ukrainian Shield: new tectonic reconstructions of the Ukrainian and Fennoscandian shields. Tectonophysics 339, 19–38.

Engel, A.E.J., Itson, S.P., Engel, C.G., Stickney, D.M., Cray, E.J., 1974. Crustal evolution and global tectonics: a petrogenetic view. Bulletin of the Geological Society of America 85, 843–858.

Evans, D.A.D., 1998. True polar wander, a supercontinent legacy. Earth and Planetary Science Letters 157, 1–8.

Evans, D.A.D., Li, Z.X., Kirschvink, J.L., Wingate, M.T.D., 2000. A high-quality mid-Neoproterozoic palaeomagnetic pole from South China with

implications for ice ages and the breakup configuration of Rodinia. Precambrian Research 1000, 313–334.
Fitzsimons, I.C.W., 2000. Grenville-age basement provinces in East Antarctica: evidence for three separate collisional orogens. Geology 28, 879–882.
Gough, D.I., 1977. The geoid and single cell mantle convection. Earth and Planetary Science Letters 34, 360–364.
Goutam, M.R., Subbarao, K.V., Prasad, C.V.R.K., Piper, J.D.A., Miggins, D.P., submitted for publication. Palaeomagnetism and $^{40}Ar/^{39}Ar$ geochronology of Proterozoic mafic dykes from the southern margin of the Cuddapah Basin, India.
Gurnis, M., Torsvik, T.H., 1994. Rapid drift of large continents during the late Precambrian and Palaeozoic: palaeomagnetic constraints and dynamic models. Geology 22, 1023–1206.
Halliday, A.N., Graham, C.M., Aftalion, M., Dymoke, P.L., 1989. The depositional age of the Dalradian Supergroup: U–Pb and Sm–Nd isotopic studies of the Tayvallich Volcanics, Scotland. Journal of the Geological Society of London 146, 3–6.
Halls, H.C., Wingate, M.T.D., 2001. Palaeomagnetic pole from the Yilgarn B (YB) dykes of Western Australia: no longer relevant to Rodinia reconstructions. Earth and Planetary Science Letters 187, 39–53.
Hanmer, S., Corrigan, D., Pehrsson, S., Nadeau, L., 2000. SW Grenville Province, Canada: the case against post-1.4 Ga accretionary tectonics. Tectonophysics 319, 33–51.
Harris, N.B.W., Gass, I.G., 1981. Significance of contrasting magmatism in North East Africa and Saudi Arabia. Nature 289, 394–396.
Higgins, M.D., van Breemen, O., 1998. The age of the Sept Îles layered mafic intrusion, Canada: implications for the Late Neoproterozoic/Cambrian history of southeastern Canada. Journal of Geology 106, 421–432.
Hoffman, P.F., 1991. Did breakout of Laurentia turn Gonwanaland inside out? Science 252, 1409–1412.
Holser, W.T., 1977. Catastrophic chemical events in the history of the oceans. Nature 267, 403–408.
Hutchinson, R.W., 1981. Mineral deposits as guides to supracrustal evolution. In: O'Connell, R.J., Fyfe, W.S. (Eds.), Evolution of the Earth. Geodynamics Series, vol. 5. American Geophysical Union, pp. 120–140.
Idnurm, M., Giddings, J.W., 1995. Palaeoproterozoic–Neoproterozoic North America–Australia link: new evidence from palaeomagnetism. Geology 23, 149–152.
Irving, E., McGylnn, J.C., 1976. Proterozoic magnetostratigraphy and the tectonic evolution of Laurentia. Philosphophical Transactions of the Royal Society of London, A 280, 243–265.
Kimura, H., Matsumoto, R., Yoshitaka, K., Bahaeddin, H., Zibasereshi, H., 1997. The Vendian–Cambrian $\delta^{13}C$ record, North Iran: evidence for overturning of the ocean before the Cambrian Explosion. Earth and Planetary Science Letters 147, E1–E7.
Kirschvink, J.L., Ripperdan, R.L., Evans, D.A.D., 1997. Evidence for a large-scale reorganisation of Early Cambrian continental landmasses by inertial interchange true polar wander. Science 277, 541–545.
Klootwijk, C.T., 1980. Early Palaeozoic palaeomagnetism in Australia. Tectonophysics 64, 249–332.
Knoll, A.H., Hayes, J.M., Kaufman, J., Swett, K., Lambert, I.B., 1986. Secular variation in carbon isotope ratios from Upper Proterozoic successions of Svalbard and East Greenland. Nature 321, 832–838.
Le Pichon, X., Huchon, P., 1984. Geoid, Pangaea and convection. Earth and Planetary Science Letters 67, 123–135.
Li, Z.X., Powell, C.McA., 1993. Late Proterozoic to Early Palaeozoic palaeomagnetism and the formation of Gondwanaland. Gondwana Eight. Balkema, Rotterdam, pp. 9–21.
Li, Z.-X., Zhang, L., Powell, C.McA., 1995. South China in Rodinia: part of the missing link between Australia–East Antarctica and Laurentia? Geology 23, 4077–4410.
Li, Z.X., Evans, D.A.D., Zhang, S., 2004. A 90° spin on Rodinia: possible causal links between the Neoproterozoic supercontinent, superplume, true polar wander and low-latitude glaciation. Earth and Planetary Science Letters 220, 409–421.
Liu, C., Wang, Q.C., Liu, H.S., 1984. Palaeomagnetic results from Early and Middle Proterozoic in Taihangshan Region. Geologica Scientia Sinica 4, 455–459.
Magaritz, M., Holser, W.T., Kirschvink, J.L., 1986. Carbon-isotope events across the Precambrian/Cambrian boundary on the Siberian Platform. Nature 320, 258–259.
McLennan, S.M., Taylor, S.R., 1983. Continental freeboard sedimentation rates and growth of continental crust. Nature 306, 169–172.
McMenamin, M.A.S., McMenamin, D.L., 1990. The Emergence of Animals: The Cambrian Breakthrough. Columbia University Press, New York. 217 pp.
McWilliams, M.O., Dunlop, D.J., 1978. Grenville palaeomagnetism and Tectonics. Canadian Journal of Earth Sciences 15, 687–695.
Meert, J.G., 1999. A palaeomagnetic analysis of Cambrian true polar wander. Earth and Planetary Science Letters 168, 131–144.
Meert, J.G., 2003. A synopsis of events related to the assembly of eastern Gondwana. Tectonophysics 362, 1–40.
Meert, J.G., Torsvik, T.H., 2003. The making and unmaking of a supercontinent: Rodinia revisited. Tectonophysics 375, 261–288.
Moores, E.M., 1991. SW US–East Antarctica (SWEAT) connection: a hypothesis. Geology 19, 425–428.
Mound, J., Mitrovica, J., 1998. True polar wander as a mechanism for second-order sea-level variations. Science 279, 534–537.
Nelson, D.R., Trendall, A.F., Altermann, W., 1999. Chronological correlations between the Pilbara and Kaapvaal Cratons. Precambrian Research 97, 165–189.
Nevanlinna, H., Pesonen, L.J., 1983. Late Precambrian Keweenawan asymmetric polarities as analysed by axial offset dipole geomagnetic field models. Journal of Geophysical Research 88, 645–688.
Onstott, T.C., Hargraves, R.B., 1981. Proterozoic transcurrent tectonics: evidence from comparison of palaeomagnetic data from Venezuela and Africa. Nature 289, 131–136.
Patchett, J.P., Bylund, G., 1977. Age of Grenville Belt magnetisations: Rb–Sr and palaeomagnetic evidence from Swedish dolerites. Earth and Planetary Science Letters 35, 92–104.
Patchett, J.P., Bylund, G., Upton, B.G.J., 1978. Palaeomagnetism and the Grenville Orogeny: new Rb–Sr ages from dolerites in Canada and Greenland. Earth and Planetarey Science Letters 40, 349–364.
Pesonen, L.J., Elming, S.-A., Mertanen, S., Pisarevsky, S., D'Agrella-Filho, M.S., Meert, J.G., Schmidt, P.W., Abrhamsen, N., Bylund, G., 2003. Palaeomagnetic configuration of continents during the Proterozoic. Tectonophysics 375, 289–324.
Pimental, M.M., Fuck, R.A., Botelho, N.F., 1999. Granites and the geodynamic history of the Neoproterozoic Brazilia belt, Central Brazil: a review. Lithos 46, 463–483.
Piper, J.D.A., 1980a. Analogous Upper Proterozoic apparent polar wander loops. Nature 283, 845–847.
Piper, J.D.A., 1980b. Palaeomagnetic study of the Swedish Rapakivi suite: Proterozoic tectonics of the Baltic Shield. Earth and Planetary Science Letters 46, 443–461.
Piper, J.D.A., 1982. The Precambrian palaeomagnetic record: the case for the Proterozoic Supercontinent. Earth and Planetary Science Letters 59, 61–89.
Piper, J.D.A., 1983a. Dynamics of the continental crust in Proterozoic times. Geological Society of America Memoir 161, 11–34.
Piper, J.D.A., 1983b. Proterozoic palaeomagnetism and single continent plate tectonics. Geophysical Journal of the Royal Astronomical Society 74, 163–197.
Piper, J.D.A., 1987. Palaeomagnetism and the Continental Crust. John Wiley, New York. 434 pp.
Piper, J.D.A., 1990. The quasi-rigid premise in Precambrian tectonics. Earth and Planetary Science Letters 107, 559–569.
Piper, J.D.A., 1992. The palaeomagnetism of major (Middle Proterozoic) igneous complexes, South Greenland and the Gardar apparent polar wander track. Precambrian Research 54, 153–172.
Piper, J.D.A., 1994. Palaeomagnetism of the Mesoproterozoic Grønnedal–Ika alkaline complex, South Greenland. Precambrian Research 69, 51–60.
Piper, J.D.A., 1995. The palaeomagnetism of middle Proterozoic dyke swarms of the Gardar Province and Mesozoic dykes in South Greenland. Geophysical Journal International 120, 339–355.
Piper, J.D.A., 2000. The Neoproterozoic Supercontinent: Rodinia or Palaeo-pangaea? Earth and Planetary Science Letters 176, 131–146.
Piper, J.D.A., 2003. Consolidation of continental crust in late Archaean–Early Proterozoic times: a palaeomagnetic test. Gondwana Research 6 (3), 435–448.

Piper, J.D.A., 2004. Discussion on "The making and unmaking of a supercontinent: Rodinia revisited" by J.G.Meert and T.H.Torsvik, Tectonophysics, 375 (2003) 261–288. Tectonophysics 383, 91–97.
Piper, J.D.A., in press. Uplift and Cooling Magnetisation Record in the Bamble and Telemark Terranes, Sveconorwegian Province: Neoproterozoic configuration of the Laurentian and Fennoscandian Shields, Precambrian Research.
Piper, J.D.A., Darabi, M.H., 2005. Palaeomagnetic study of the (Late Mesoproterozoic) Torridon Group, NW Scotland: age, magnetostratigraphy, tectonic setting and magnetic overprinting by Caledonian Orogeny. Precambrian Research 142, 45–81.
Piper, J.D.A., Zhang, Q.R., 1997. Palaeomagnetism of Neoproterozoic glacial rocks of the Huabei Shield: the North China Block in Gondwana. Tectonophysics 283, 145–171.
Piper, J.D.A., Thomas, D.N., Share, S., Zhang, Q.-R., 1999. The palaeomagnetism of Mesoproterozoic Eriksfjord Group red beds, South Greenland: multiphase remagnetisation during the Gardar and Grenville episodes. Geophysical Journal International 136, 739–756.
Pisarevsky, S.A., Bylund, G., 1998. Neoproterozoic palaeomagnetic directions in rocks from a key section of the Protogine Zone, Southern Sweden. Geophysical Journal International 133, 185–200.
Powell, C. McG., 1995. Are Neoproterozoic glacial deposits preserved on the margins of Laurentia related to the fragmentation of two supercontinents? Comment. Geology 23, 1053–1054.
Powell, C. McG., Pisarevsky, S.A., 2002. Late Neoproterozoic assembly of East Gondwana. Geology 30, 3–6.
Powell, C. McG., Li, Z.X., McElhinny, M.W., Meert, J.G., Park, J.K., 1993. Palaeomagnetic constraints on timing of the Neoproterozoic break up of Rodinia and the Cambrian formation of Gondwana. Geology 21, 889–892.
Quade, J., Roe, L., DeCelles, P.G., Ojha, T.P., 1997. The late Neogene $^{87}Sr/^{86}Sr$ record of lowland Himalayan rivers. Science 276, 1828–1831.
Rogers, J.J.W., 1996. A history of continents in the past three billion years. Journal of Geology 104, 91–107.
Rogers, J.J.W., Santosh, M., 2004. Continents and Supercontinents. Oxford University Press. 289 pp.
Ronov, A.B., 1968. Probable changes in the composition of sea water during the course of geological time. Sedimentology 10, 25–43.
Schmidt, P.W., Williams, G.E., 2003. Reversal asymmetry in Mesoproterozoic overprinting of the 1.88 Ga Gunflint Formation, Ontario, Canada: non-dipole effects or apparent polar wander? Tectonophysics 377, 7–32.
Sears, J.W., Price, R.A., 1978. The Siberian Connection: a case for the Precambrian separation of the North American and Siberian cratons. Geology 6, 267–270.
Sears, J.W., Price, R.A., 2000. New look at the Siberian connection: no SWEAT. Geology 28, 423–426.
Smethurst, M.A., Khramov, A.N., Torsvik, T.H., 1998. The Neoproterozoic and Palaeozoic palaeomagnetic data from the Siberian Platform: from Rodinia to Pangaea. Earth Science Reviews 43, 1–24.
Stearn, J.E.F., Piper, J.D.A., 1984. Palaeomagnetism of the Sveconorwegian mobile belt of the Fennoscandian Shield. Precambrian Research 23, 210–246.
Steinberger, B., O'Connell, R.J., 2002. The convective mangle flow signal in rates of true polar wander. In: Mitrovica, J., Vermeersen, B. (Eds.), Ice Sheets, Sea Level and the Dynamic Earth, vol. 29. American Geophysical Union, pp. 233–256.a.
Stern, R.J., 1994. Arc assembly and continental collision in the Neoproterozoic East Africa Orogen: implications of the consolidation of Gondwanaland. Annual Review of Earth and Planetary Science 22, 319–351.
Thomas, D.N., Piper, J.D.A., 1992. A revised magnetostratigraphy for the Mid-Proterozoic Gardar lava succession, South Greenland. Tectonophysics 201, 1–16.
Torsvik, T.H., Carter, L.M., Ashwal, L.D., Bhushanm, S.K., Pandit, M.K., Jamtveit, B., 2001a. Rodinia refined or obscured; palaeomagnetism of the Malani Igneous suite (NW India). Precambrian Research 108, 319–333.
Torsvik, T.H., Ashwal, L.D., Tucker, R.D., Eide, E.A., 2001b. The birth of the Seychelles microcontinent. Precambrian Research 110, 47–59.
Trompette, R., 1997. Neoproterozoic (~600 Ma) aggregation of western Gondwana: a tentative scenario. Precambrian Research 82, 101–112.
Veizer, J., 1989. Strontium isotopes in seawater through time. Annual Reviews of Earth and Planetary Science 17, 141–187.
Warnock, A.C., Kodama, K.P., Zeitler, P.K., 2000. Using thermochronometry and low-temperature demagnetisation to accurately date Precambrian palaeomagnetic poles. Journal of Geophysical Research 105, 19435–19453.
Wegener, A., 1923. The Origin of Continents and Oceans. Methuen, London. 212 pp.
Weil, A.B., Van der Voo, R., MacNiocaill, C., Meert, J.G., 1998. The Proterozoic supercontinent Rodinia: palaeomagnetically derived reconstructions for 1100 to 800 Ma. Earth and Planetary Science Letters 154, 13–24.
Wingate, M.T.D., 1998. A palaeomagnetic test of the Kaapvaal–Pilbara (Vaalbara) connection at 2.78 Ga. South African Journal of Geology 101, 257–274.
Wingate, M.T.D., Pisarevsky, S.A., Evans, D.A.D., 2002. Rodinia connections between Australia and Laurentia: no SWEAT, no AUSWUS? Terra Nova 14, 121–128.
Yale, L.B., Carpenter, S.J., 1998. Large igneous provinces and giant dike swarms: proxies for supercontinent cyclicity and mantle convection. Earth and Planetary Science Letters 163, 109–122.
Young, G.M., 1992. Late Proterozoic stratigraphy and the Canada–Australia connection. Geology 20, 215–218.
Zegers, T.E., de Wit, M.J., Dann, J., White, S.H., 1998. Vaalbara, Earth's oldest assembled continent? A combined structural, geochronological and palaeomagnetic test. Terra Nova 10, 250–259.
Zhang, H.M., 1995. China Precambrian palaeomagnetic data list. Acta Geoscientia Sinica 4, 441–448.
Zhang, Q.-R., Piper, J.D.A., 1997. Palaeomagnetic study of Neoproterozoic glacial rocks of the Yangzi Block: palaeolatitude and configuration of South China in the late Proterozoic Supercontinent. Precambrian Research 85, 173–199.
Zhang, H.M., Zhang, W.Z., Elston, D.P., 1991. Palaeomagnetic study of Middle and Late Proterozoic rocks in Jixian, North China. Chinese Journal of Geophysics 34, 631–647.
Zhou, X., Hu, S., Ren, S., Li, J., 1993. Isochronological constraints to multistage tectonic evolution of the continental crust in southeastern China. In: Li, J. (Ed.), Geophysical Structure and Geological Evolution of Continental Lithosphere in Southeastern China. Metallurgical Industry Press, Beijing, pp. 66–69.
Zhou, C., Tucker, R., Xiao, S., Peng, Z., Yuan, X., Chen, Z., 2004. New constraints on the ages of Neoproterozoic glaciations in South China. Geology 32, 437–440.



John Piper graduated in geology from the University of Bristol and undertook a PhD at Imperial College, London, on palaeomagnetism and magnetic interpretation in Iceland. After three years of postdoctoral work at the Institute of African Geology at the University of Leeds where he worked on palaeomagnetism of Precambrian rocks, he joined the Geomagnetism Laboratory at the University of Liverpool in 1973 where he has been based ever since. His main field of investigation has been into the applications of palaeomagnetism to the study of Precambrian geology and continental reconstruction. In the pursuit of this he has undertaken investigations in Greenland, China, India, Norway and Sweden as well as on home ground in the Hebridean Craton of northwest Scotland. Links with Turkish universities and the Chinese Academy of Sciences have also enabled him to apply palaeomagnetism to the study of neotectonics in the Alpine–Himalayan orogenic belt.